

An FcRn-targeted mucosal vaccine against SARS-CoV-2 infection and transmission

Received: 12 September 2023

Accepted: 21 October 2023

Published online: 06 November 2023

 Check for updates

Weizhong Li¹, Tao Wang¹, Arunraj M. Rajendrakumar^{1,2}, Gyanada Acharya¹, Zizhen Miao¹, Berin P. Varghese¹, Hailiang Yu¹, Bibek Dhakal¹, Tanya LeRoith³, Athira Karunakaran², Wenbin Tuo² & Xiaoping Zhu¹✉

SARS-CoV-2 is primarily transmitted through droplets and airborne aerosols, and in order to prevent infection and reduce viral spread vaccines should elicit protective immunity in the airways. The neonatal Fc receptor (FcRn) transfers IgG across epithelial barriers and can enhance mucosal delivery of antigens. Here we explore FcRn-mediated respiratory delivery of SARS-CoV-2 spike (S). A monomeric IgG Fc was fused to a stabilized spike; the resulting S-Fc bound to S-specific antibodies and FcRn. Intranasal immunization of mice with S-Fc and CpG significantly induced antibody responses compared to the vaccination with S alone or PBS. Furthermore, we intranasally immunized mice or hamsters with S-Fc. A significant reduction of virus replication in nasal turbinate, lung, and brain was observed following nasal challenges with SARS-CoV-2 and its variants. Intranasal immunization also significantly reduced viral airborne transmission in hamsters. Nasal IgA, neutralizing antibodies, lung-resident memory T cells, and bone-marrow S-specific plasma cells mediated protection. Hence, FcRn delivers an S-Fc antigen effectively into the airway and induces protection against SARS-CoV-2 infection and transmission.

SARS-CoV-2, a virus causing the COVID-19 pandemic, is highly infectious, circulates rapidly worldwide, and mutates constantly. The SARS-CoV-2 variants include Alpha (B.1.1.7), Beta (B.1.351), Gamma (P.1), Delta (B.1.617.2), and Omicron (B.1.1.529, BA.4/BA.5, XBB.1.5). These variants evade the immunity induced by current vaccines and prior infections. Through the receptor-binding domain (RBD) of its spike (S) protein, SARS-CoV-2 binds to the angiotensin-converting enzyme 2 (ACE2). The S protein undergoes a structural change upon binding and is cleaved by host proteases, such as the transmembrane serine protease 2 (TMPRSS2), allowing it to fuse with the cellular membrane for host cell entry¹. Because of its vital role in mediating receptor binding and infection initiation, the S protein is the primary target for developing vaccines².

SARS-CoV-2 can be shed from individuals with asymptomatic infections and spread predominantly through droplets and airborne aerosols³. The virus first enters the nose or mouth and replicates

within epithelial cells of the nasopharynx, causing an upper respiratory infection. Hence, the nasal mucosa and nasopharynx are the primary sites of exposure to SARS-CoV-2 before dissemination to the lungs and other tissues/organs⁴. The currently authorized intramuscular vaccines can effectively prevent severe diseases and deaths caused by COVID-19. However, they cannot effectively elicit protective mucosal immunity in the upper respiratory tract⁵⁻⁷. This shortcoming allows opportunistic breakthrough infections in those who received vaccinations⁸. Hence, the SARS-CoV-2 can linger in the nasal mucosa even after clearing infection in the lungs in vaccinated individuals. The emergence of the SARS-CoV-2 variants, especially the Omicron, exacerbates the situation. This evolution of SARS-CoV-2 necessitates a safe and protective mucosal vaccine to block the viral entry and reduce or eliminate the viral spread, thus preventing lung and systemic infection and breakthrough infection. Nasal-spray vaccines can elicit local secretory IgA antibodies

¹Division of Immunology, Virginia-Maryland College of Veterinary Medicine, University of Maryland, College Park, MD 20742, USA. ²Animal Parasitic Diseases Laboratory, ARS, United States Department of Agriculture, Beltsville, MD 20705, USA. ³Department of Biomedical Sciences and Pathobiology, Virginia-Maryland College of Veterinary Medicine, Virginia Tech University, Blacksburg, VA, USA. ✉e-mail: xzhu1@umd.edu

and resident T and B cell responses in the upper respiratory tract and the lungs^{6,9,10}.

Epithelial cells lining the respiratory tract form a mucosal barrier. The neonatal Fc receptor (FcRn) binds to the Fc portion of IgG and mediates the transfer of IgG across the epithelial cells, a function essential to IgG distribution and homeostasis^{11–14}. Typically, FcRn shows a pH-dependent IgG binding, with a preference to bind IgG at acidic pH (6.0–6.5)¹⁴. Generally, the FcRn-IgG on the cell surface or in the endosome under acidic conditions goes through a non-degradative vesicular transport pathway within epithelial cells. Consequently, FcRn transports its bound IgG across the mucosal barrier and then releases it into the lumen or submucosa upon exposure to physiological pH¹⁴. Through binding, FcRn also extends the half-life of IgG by reducing lysosomal degradation in cells, such as endothelial cells¹⁵.

The vaccine must be administered locally in the respiratory tract to establish respiratory immunity with resident memory of T and B cells in the lungs^{16,17}. In this study, we determine the ability of FcRn to deliver an intranasally-administered SARS-CoV-2 S antigen and induce protective mucosal and systemic immunity to SARS-CoV-2 infection. We define protective immune responses and mechanisms relevant to this nasal vaccination in the mouse and hamster models. Our results show that FcRn-mediated nasal delivery of a prefusion-stabilized SARS-CoV-2 S antigen induces secretory IgA Abs in the nasal lavage and high levels of long-lasting Ab and T-cell responses. Our nasal vaccine confers durable protection against SARS-CoV-2 infection and airborne transmission.

Results

Expression and characterization of SARS-CoV-2 S-Fc proteins

To target antigen to FcRn, we expressed a monomeric human IgG1 Fc fused to a prefusion-stabilized, soluble form of S, which contained an R685A mutation at the furin cleavage site, an R815A mutation at S2' cleavage site, and 2P conversions (Fig. 1a) along with the T4 fibrin trimerization¹⁸. We also removed the C1q binding site in IgG1 Fc.

We showed that the soluble S or S-Fc protein was secreted from the stable CHO cells (Fig. 1b). Since IgG only binds to FcRn at acidic pH¹⁴, we determined if the S-Fc portion binds to FcRn at either pH 6.0 or 7.4. As shown in Fig. 1c, S-Fc interaction with both human (Fig. 1c) and mouse (Fig. 1c) FcRn/ β 2m was detected at pH 6.0 condition. Since hamster FcRn/ β 2m is not available, we generated biotinylated hamster FcRn/ β 2m (Fig. S1d). We found the S-Fc bound to hamster FcRn/ β 2m like human or mouse FcRn/ β 2m did (Fig. 1c). However, the binding of the S to human, mouse, and hamster FcRn/ β 2m protein was barely detectable (Fig. 1c). To further show whether the S-Fc binds to Fc γ RI (CD64), we also produced biotinylated hamster Fc γ RI (Fig. S1e). As expected, the S protein did not bind to mouse, human, and hamster Fc γ RI (Fig. 1d). As shown in Fig. 1d, the S-Fc, human IgG1, or hamster IgG2 bound to human and hamster Fc γ RI similarly in an ELISA assay. However, the S-Fc did not bind mouse Fc γ RI with high affinity (Fig. 1d), although mouse IgG was shown to bind mouse Fc γ RI strongly. This result could be explained by the fact that human IgG1 does not interact with mouse Fc γ RI with high affinity¹⁹.

We next determined if the S portion of the S-Fc binds to human ACE-2. In an ELISA assay, the S-Fc and S protein bound to human ACE-2 similarly (Fig. 1e), indicating the Fc fusion doesn't affect the conformation of S in the S-Fc protein. As a negative control, RSV F protein with or without Fc-fusion did not bind to human ACE-2 (Fig. 1e). In contrast to an RSV-F specific mAb (D25), the S-Fc could not bind to human or mouse C1q protein (Fig. 1f) *in vitro*. We further wanted to know if the S portion of the S-Fc interacts with convalescent serum Abs compared to the S alone. Normal human sera from different healthy donors were used as a negative control. Indeed, the sera from convalescent COVID-19 patients (Fig. S2a) were able to recognize both

purified S-Fc (solid lines) and S (dashed lines) proteins with varying binding efficiencies. Most importantly, S-Fc and S showed the same binding levels for each tested serum sample, indicating that Fc-fusion with S didn't alter its conformation. Normal sera (Fig. S2b) from healthy individuals showed no binding activity. The results were further confirmed by the interactions of both S-Fc and S with various spike-specific mAbs (Fig. S2c, d). Together, the S portion of the S-Fc protein maintains the correct conformational structure, allowing for binding to the ACE-2 and S-specific Abs, and possesses the function to engage with FcRn and human or hamster Fc γ RI.

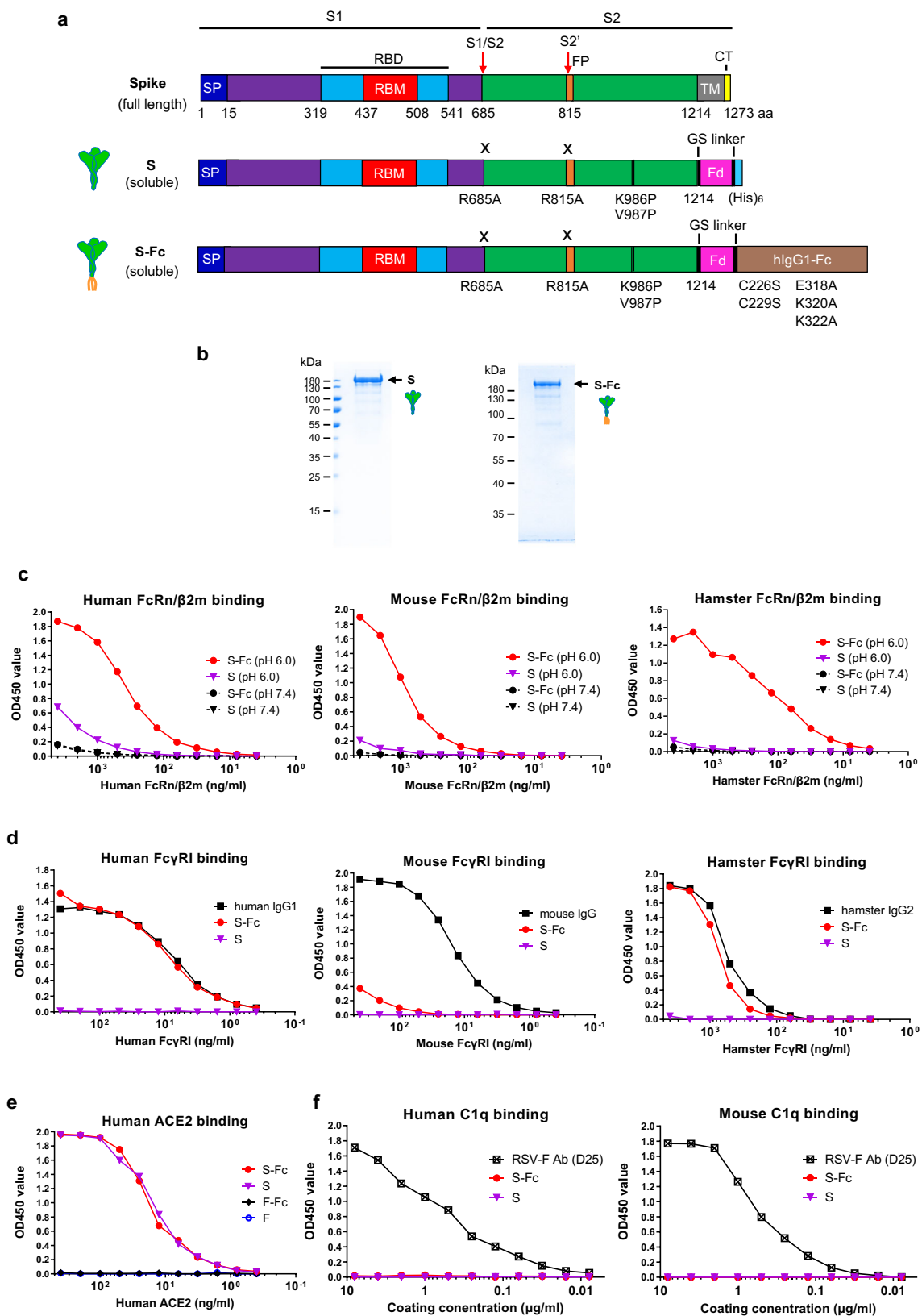
FcRn-mediated respiratory delivery enhances S-specific immune responses

We tested whether FcRn-dependent transport augments the immune responses to the S protein. C57BL/6 mice were *i.n.* immunized with 10 μ g of S-Fc, S protein (equal molar amount), or PBS in 10 μ g CpG adjuvant, the mice were boosted after 2 weeks (Fig. 2a). FcRn-knockout (KO) mice were used as a control to test the FcRn-mediated immunity enhancement. Using S protein alone allowed us to evaluate FcRn-independent effects *in vivo* and determine the magnitude of enhanced immune responses conferred by targeting the S-Fc to FcRn. As shown in Fig. 2, significantly higher titers of total serum IgG (Fig. 2b) were detected in the S-Fc immunized WT mice compared with the S-Fc-immunized FcRn KO, the S-immunized or PBS-treated WT mice. Moreover, sera from the S-Fc immunized mice exhibited much stronger neutralizing activity than the control groups (Fig. 2c). Likewise, the S-Fc induced higher levels of IgG (Fig. 2d, e) and IgA (Fig. 2f, g) Abs in nasal washes (Fig. 2d, f) and bronchoalveolar lavage fluids (BAL) (Fig. 2e, g) than those of the WT mice immunized by the S alone, PBS or the FcRn KO mice immunized by the S-Fc. Since human IgG1 Fc was utilized in producing S-Fc, as expected, low levels of anti-Fc IgG were detected in the mouse sera after the *i.n.* boost (Fig. S2e).

Activated B cells can differentiate into plasma cells that secrete antibodies at a high rate and reside in niches within the bone marrow. To determine whether antigen targeting to FcRn also elicits plasma cells that secrete S-specific Abs, the number of IgG-secreting plasma cells in the bone marrow was measured 8 months after the boost by ELISpot. High numbers of S-specific IgG-secreting cells were present in the bone marrow of mice immunized with S-Fc compared with other groups (Fig. 2h). To show whether the increased IgG-secreting plasma cells correspond to a rise in Ab production and maintenance, IgG Abs in the sera were measured 8 months after the boost. High titers of S-specific IgG Abs were maintained in mice immunized with the S-Fc, but not the S alone (Fig. 2i). Also, a significant level of S-specific IgA or IgG was present in the nasal washes or BAL of mice immunized with S-Fc compared with other groups 14 months later (Fig. S3a–d). Immunization with the S-Fc was more effective than immunization with S alone, indicating that S-specific Abs persisted much longer after FcRn-targeted mucosal immunization. Our data demonstrate that an Fc-fused, soluble, prefusion-stabilized S protein delivered through FcRn is much more potent in triggering S-specific Ab responses.

Intranasal immunization by S-Fc protects mice from SARS-CoV-2 infection

Human ACE2 transgenic mice are highly susceptible to SARS-CoV-2 intranasal challenges when high virus doses are used²⁰. In the study, hACE2 mice were *i.n.* immunized with 10 μ g of S-Fc or PBS in 10 μ g CpG and boosted in a 2-week interval (Fig. 3a). We confirmed that significantly higher titers of serum IgG (Fig. 3b) and neutralizing antibodies (nAbs) (Fig. 3c) were detected in the hACE2 mice *i.n.* immunized with the S-Fc when compared with PBS-treated mice. To test whether the immune responses elicited by the intranasal (*i.n.*) vaccination with the S-Fc provide protection, we *i.n.* challenged all immunized mice with a lethal dose (2.5×10^4 TCID₅₀) of ancestral SARS-CoV-2 virus 2–3 weeks after the boost (Fig. 3a). Mice were monitored



and weighed daily for 14 days. All mice in the control groups exhibited rapid weight loss following the challenge, either succumbing to infection within 8 days post-infection (dpi) or being subjected to euthanasia. In contrast, the S-Fc-immunized mice did not experience significant body-weight loss (Fig. 3d) and had complete protection with significantly higher survival rates (100%) than those of the PBS

control group (Fig. 3e). As expected, all the PBS-treated mice had high virus loads in the lung at 5 dpi. In contrast, a significant reduction of virus load in the nasal turbinates, lungs, and brain tissue was seen in the S-Fc immunized mice when compared to the control animals (Fig. 3f). We also challenged the hACE2 mice that were i.n. immunized with the S-Fc protein (Fig. S3g) derived from the Omicron XBB.1.5 variant.

Fig. 1 | Expression and characterization of the Spike and prefusion Spike-Fc (S-Fc) protein. **a** Schematic illustration of the full-length protein sequence of SARS-CoV-2 Spike. SP: signal peptide; RBD: receptor binding domain; TM: transmembrane domain; CT: cytoplasmic tail. Graphic design of the fusion of SARS-CoV-2 Spike with the T4 fibrin foldon domain (Fd) to create a soluble, prefusion-stabilized, and trimeric Spike protein. Mutations were made in the SARS-CoV-2 (strain USA/WA1/2020) spike by replacing Arg 685 and Arg 815, respectively, with an Ala residue to remove the cleavage site and replacing Lys 986 and Val 987, respectively, with a Pro residue to create a prefusion-stabilized form. The diagram demonstrates the fusion of a SARS-CoV-2 Spike with the T4 fibrin foldon domain and human Fcγ1 to create a prefusion-stabilized and trimeric S-Fc fusion protein. Mutations were also made in the Fcγ1 fragment by replacing Cys 226 and Cys 229, respectively, with a Ser residue to abolish Fc dimerization, and replacing Glu 318 Lys 320 Lys 322 with

Ala residues to remove the complement C1q binding site. **b** The S and S-Fc fusion proteins were purified from the stable CHO cell lines. The soluble S and S-Fc proteins were purified by anti-His and Protein A affinity chromatography, respectively, subjected to SDS-PAGE gel electrophoresis under reducing conditions and visualized with Coomassie blue staining. The figure is a representative result from three independently-repeated experiments. **c–f** Test of the S-Fc binding to human, mouse, or hamster FcRn/β2m; human, mouse, or hamster FcγRI; human ACE2; and human or mouse C1q. The ELISA determined the specific binding. The purified S protein was used as a positive control for ACE2 binding and a negative control for FcRn/β2m or FcγRI binding. Respiratory syncytial virus (RSV) protein F alone or Fc-fused F proteins were used as a negative control. Mouse IgG, human IgG1, hamster IgG2, and a mAb (D25) against RSV F protein were used as the positive control, respectively. Source data are provided as a Source data file.

Similarly, a significant reduction of XBB.1.5 virus load in the lungs was seen in the XBB.1.5 S-Fc immunized mice compared to the PBS control animals (Fig. S3h). Interestingly, brain tissues exhibited the highest levels of virus load in the PBS control mice at 5 dpi. Therefore, the S-Fc-immunized hACE2 mice essentially contained viral replication in tissues/organs of the viral entry and prevented the viral spreading to other tissues/organs.

Lungs were collected at 5 dpi to show protection for further histopathological analysis. The lungs of uninfected mice were used as normal control (Fig. 3g). Before the virus challenge, no apparent alterations were observed in the lung structure and histology of the S-Fc immunized mice and normal mice, suggesting that the S-Fc did not induce inflammation. In contrast, we found focal inflammatory cell infiltration, pneumonia, peribronchiolitis, and perivascularitis in the lungs of PBS control mice after virus infection (Fig. 3g). The alveolitis was not observed. Hence, the mice immunized with S-Fc had a significantly lower lung inflammation score than those in the PBS group (Fig. 3h, $p < 0.05$). We also found that i.n. immunization with the S-Fc protected the aged hACE2 mice from lethal SARS-CoV-2 infection (Fig. S4a–f; Supplementary note 1) and elicited durable protection in hACE2 mice (Fig. S4g–j; Supplementary note 2). These findings demonstrate that FcRn-mediated delivery of the S-Fc confers significant protection against lethal SARS-CoV-2 challenge, resulting in decreased mortality, viral replication, and pulmonary inflammation in a hACE2 mouse model.

Intranasal immunization with S-Fc protects infections of SARS-CoV-2 variants

The SARS-CoV-2 is rapidly evolving via mutagenesis, significantly impacting transmissibility, morbidity, reinfection, and mortality while lengthening the pandemic. Since the S portion of the S-Fc is derived from ancestral SARS-CoV-2, we wanted to determine the effectiveness and neutralizing activity elicited by the S-Fc vaccine against Delta and Omicron variants. First, we i.n. immunized hACE2 mice twice with 10 μg of S-Fc adjuvanted in 10 μg CpG (Fig. 4a) and tested the protection against the SARS-CoV-2 Delta strain. Most immunized mice developed nAbs against the Delta strain after the boost (Fig. S3e, $p < 0.01$). To show protection, we challenged all immunized mice with a lethal dose (2.5×10^4 TCID₅₀) of the Delta strain 17 days after the boost. All mice in the control group experienced rapid weight loss (Fig. 4b), labor breathing, and ataxia before finally dying from the viral infection or were humanely euthanized. In contrast, the S-Fc-immunized hACE2 mice did not show significant body-weight loss (Fig. 4b) or clinical signs. The majority (83.3%) of the S-Fc-immunized mice survived, which was significantly higher than the survival rates of the PBS control group, where all mice died from Delta virus infection (Fig. 4c). Furthermore, we measured viral replication in the nasal turbinate, lung, and brain tissues 6 dpi (Fig. 4d). We were able to detect live Delta virus in the nasal turbinates, lungs, and brain tissues of the PBS control mice. Still, we failed to find any live virus in the S-Fc-

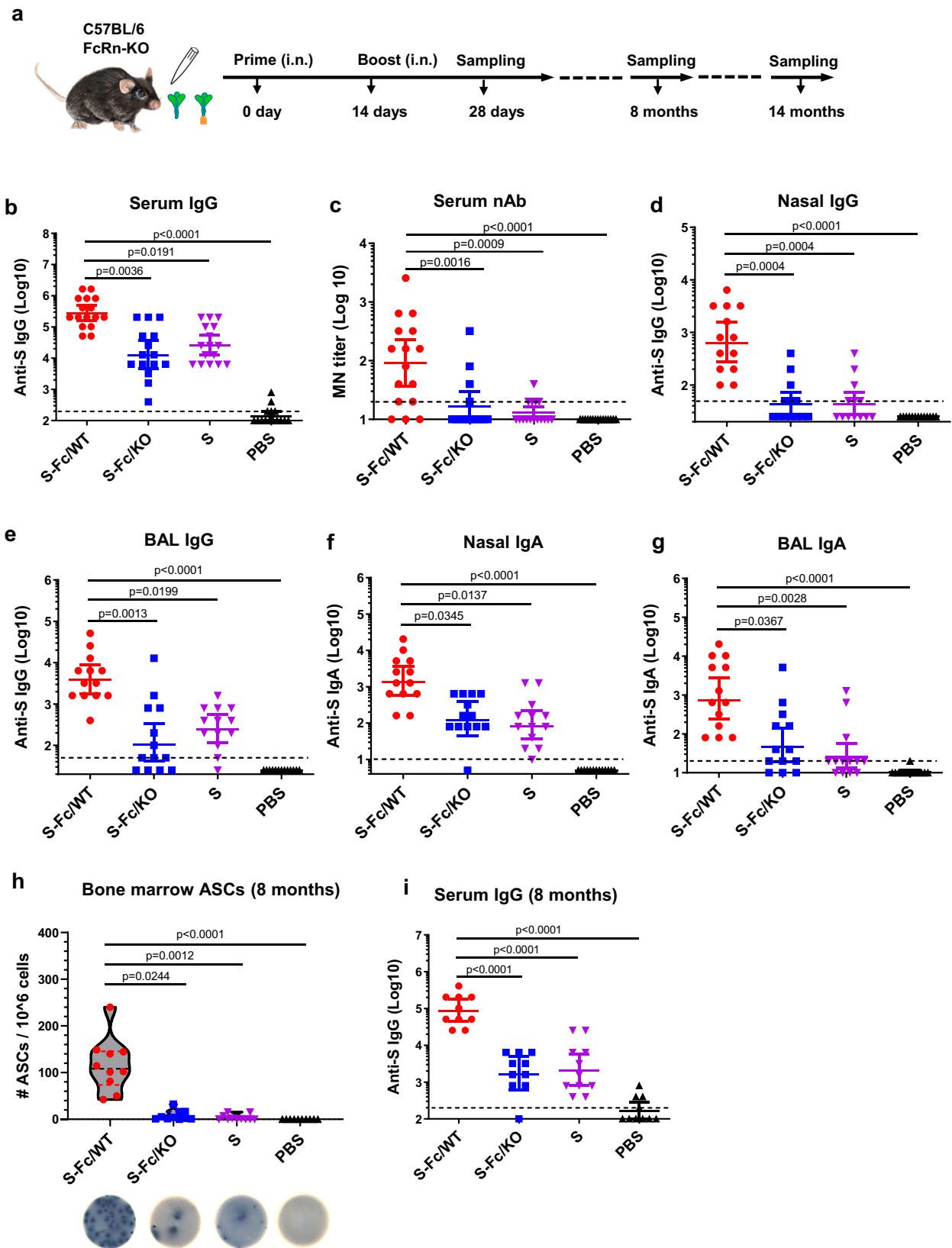
immunized animals' nasal turbinates and lung tissues (Fig. 4d). Only one mouse in the S-Fc-immunized group showed reduced virus load for brain samples.

In contrast, the others had no virus detected. Additionally, no prominent inflammation was observed in the lungs of the S-Fc immunized mice. In contrast, focal perivascular, peribronchial inflammation and thickening of the alveolar septa were found in the lung of PBS control mice (Fig. 4e). The mice immunized with S-Fc had a significantly lower inflammatory score compared to the challenged mice in PBS control group (Fig. S3f, $p < 0.01$).

Interestingly, three i.n. immunizations were necessary to produce the Omicron-specific nAbs in the sera of most mice (Fig. 4f, g). Since the Omicron strain possesses abundant mutations in its S protein, this implies that Omicron can escape nAbs elicited by the ancestral S protein²¹. Noticeably, when the S-Fc immunized mice were challenged with a dose (1×10^6 TCID₅₀) of the Omicron B.1.1.529 strain after the 2nd boost, there was no difference in visual clinical symptoms and body-weight loss between the S-Fc-immunized and the PBS control mice throughout the experiments (Fig. 4h), which can be attributed to the low virulence of the Omicron strain in mice. We found no live Omicron virus in nasal turbinate and brain tissues (Fig. 4i, j) in all S-Fc-immunized mice at 4 and 6 dpi. For lung tissues, live Omicron virus was only identified in 2 mice immunized with S-Fc at 4 dpi at low levels (around 1030 and 22 folds of virus reduction compared to the average virus titer in PBS groups) but not 6 dpi, indicating limited viral replication in these mice. In contrast to the ancestral and Delta strains, the Omicron B.1.1.529 infection in mice did not cause body-weight loss and mortality. However, the S-Fc nasal immunization remarkably attenuated replication of the Omicron variant in the respiratory tract and the brain, substantially reducing lung inflammation in the hACE2 mice.

Intranasal immunization with S-Fc induces local immunity to viral infections

Because SARS-CoV-2 initiates its infection in the upper respiratory tract³, a nasal vaccine must elicit anti-viral IgA Abs in the nasal secretions and BAL of the lungs. First, to determine the ability of the respiratory immunization by the S-Fc to induce local humoral immune responses, we examined S-specific Abs in mucosal secretions, which were compared to mice that received intramuscular (i.m.) immunization with the same amount of the S-Fc and CpG (Fig. 5a). The nasal washes and BAL were collected 14 days following the boost and analyzed for S-specific IgA and IgG by ELISA. As shown in Fig. 5, the levels of S-specific IgA Abs significantly increased in the nasal washes and BAL (Fig. 5b, c) in the i.n. immunized mice. In contrast, the mice immunized with the S-Fc via the i.m. route showed much lower levels of S-specific IgA in both the nasal washes and BAL (Fig. 5b, c, $p < 0.0001$). The mice that were i.m. immunized with the S-Fc had higher levels of S-specific IgG in the nasal washes than that of the i.n. immunized mice (Fig. 5d, $p < 0.01$). However, both i.n. and i.m. S-Fc-



immunized mice exhibited similar levels of IgG Ab in the BAL (Fig. 5c). The mice that were i.m. immunized with the S-Fc also developed higher levels of IgG Ab in the sera than those of the i.n. immunized mice (Fig. 5d, $p < 0.01$); this may reflect the full deposit of the S-Fc protein in the tissue by the needle injection, compared to i.n. immunization, which usually results in a lower-than-desired dose.

Tissue-resident memory (TRM) T cells are found in the nasal cavity and lungs during SARS-CoV-2 infection, essential to limit disease severity and viral replication²². Thus, we next determined whether intranasal delivery of the S-Fc protein can induce TRM T cells in the lungs. The TRM T cells in the lungs were assessed 14 days after the boost by FACS (Fig. 5e and Fig. S5). Compared to the PBS control, we

Fig. 2 | FcRn-mediated respiratory immunization induces SARS-CoV-2 S-specific antibody immune responses. **a** Ten μg of S-Fc, S (with the equivalent molar number), or PBS in combination with 10 μg of CpG was i.n. administered into 6–8-week-old wild-type (WT) C57BL/6, or FcRn knockout (KO) mice. Mice were boosted 14 days after the primary immunization. Sampling was performed at the indicated time points. **b** Anti-S-specific IgG Ab levels in sera. The Ab titers were measured by coating ELISA plates with S protein. The IgG titers were measured in mouse sera ($n = 16$ for S-Fc/WT and S groups, $n = 15$ for S-Fc/KO and PBS groups). The data represent a geometric mean with 95% CI. **c** Test of neutralizing Ab activity in sera of the immunized animals. Sera from mice ($n = 16$ for S-Fc/WT and S groups, $n = 15$ for S-Fc/KO and PBS groups) were heat-inactivated and serially diluted two-fold. The ancestral SARS-CoV-2 strain (100 TCID₅₀) was added and incubated at 37°C for 1 h. The mixture was added to Vero-E6 cells and incubated at 37°C for 96 hrs. The neutralization Ab titers were determined and are expressed as the reciprocal of the highest dilution preventing the cytopathic effect (CPE). **d–g** Anti-

S-specific Ab titers in nasal washings (**d**, IgG; **f**, IgA), and BAL (**e**, IgG; **g**, IgA) of mice ($n = 13$ for each group). The data represent a geometric mean with 95% CI.

h S-specific Ab-secreting cells in the bone marrow. Bone marrow cells isolated 8 months after the boost were placed on S-coated plates and quantified by ELISpot analysis of IgG-secreting plasma cells. Data were pooled from two experiments ($n = 10$ for S-Fc/WT, S-Fc/KO, and PBS groups and $n = 11$ for S group). The graphs were plotted based on each experiment's average spot number from the duplicated wells. A violin plot with 25th, 50th, and 75th percentiles was shown. **i** Anti-S-specific IgG Ab titers in sera 8 months after the booster ($n = 10$ for S-Fc/WT, S-Fc/KO, and PBS groups and $n = 11$ for S group). The data represent a geometric mean with 95% CI. The statistical analyses were done by one-way ANOVA (Kruskal–Wallis test followed by Dunn's multiple comparisons tests) (**b–h**), and ordinary one-way ANOVA with Dunnett's multiple comparison tests (**i**). The horizontal dashed lines indicate the limit of detection (LOD). Source data are provided as a Source data file.

detected a notably higher percentage of IV-CD4⁺CD44⁺CD69⁺CD103⁺ TRM cells (Fig. 5f) and IV-CD8⁺Tet⁺CD44⁺CD69⁺CD103⁺ TRM cells (Fig. 5g) in the lungs of the i.n. immunized, but not in the i.m. immunized mice with the S-Fc. Together, these data suggest that the intranasal, but not intramuscular, immunization with the S-Fc protein induces CD4⁺ and CD8⁺ TRM cells in the lung.

Finally, to demonstrate the protective efficacy of the nasal vaccination, we challenged the i.n. or i.m. immunized hACE2 mice with the SARS-CoV-2 (2.5×10^4 TCID₅₀) (Fig. S6a). Then, we measured viral titers in nasal turbinates, throat, lungs, and brain tissues from the early to the middle phase of infection (1–4 dpi). Virus titers on 1–2 dpi in the nasal turbinates and throat of the animals who received i.n. immunizations were significantly lower than the virus titers from the animals that received i.m. immunizations (Fig. S6b, c, $p < 0.05$), respectively. Contrary to the PBS group, hACE2 mice immunized with S-Fc via either i.n. or i.m. routes showed complete inhibition of virus growth and dissemination in the lung (Fig. S6d) and brain (Fig. S6e) at 2 and 4 dpi. Overall, these data suggest that the i.n. delivery of the S-Fc vaccine induces local humoral and cellular immune responses, providing more efficacious protection in the upper respiratory tract against SARS-CoV-2 infection than the i.m. route.

Intranasal immunization with S-Fc reduces viral transmission in hamsters

SARS-CoV-2 is highly contagious; airborne transmission is a major concern in public health, as inhalation represents a primary transmission route for COVID-19. Hence, a vaccine can prevent or reduce SARS-CoV-2 airborne transmission from vaccinated individuals to unvaccinated and vice versa is highly desirable. Hamster-to-hamster²³ or hamster-to-human²⁴ transmissions of SARS-CoV-2 occur.

We first immunized hamsters and showed hamsters that were i.n. immunized with S-Fc were protected from ancestral SARS-CoV-2 infection (Fig. S7; Supplementary note 3). Hamsters that were either i.n. or i.m. immunized by the S-Fc (Fig. S7a) developed significantly higher levels of IgG (Fig. 6a) and nAb (Fig. 6b) in the sera in comparison to the PBS control hamsters. However, the hamsters that were immunized with the S-Fc via the i.n. route, compared to the i.m. route, had much higher levels of S-specific IgA Ab (Fig. 6c, $p < 0.01$). The IgG Ab (Fig. 6d) in the nasal washes didn't show big difference between i.n. and i.m. groups. To test the transmissibility, we used a unidirectional airflow chamber. Naive hamsters were exposed to the i.n. immunized hamsters that were infected with SARS-CoV-2, and vice versa (Fig. 6e). As a control, the naive hamsters were also exposed to infected naive hamsters. The i.m. immunized hamsters by the S-Fc were used as a control. Subsequently, we i.n. infected hamsters with a high titer of SARS-CoV-2 (1×10^5 TCID₅₀/hamster) to replicate a breakthrough infection (Fig. 6f). Both naive and immunized hamsters were exposed to infected immunized or naive hamsters in the unidirectional airflow chamber for 10–14 days.

As expected, all six unimmunized hamsters exposed to the SARS-CoV-2-infected unimmunized hamsters had a high titer of live virus detected in their throats, which peaked at 3–6 dpi (Fig. 6f, group 1), indicating that SARS-CoV-2 infection and airborne transmission was successful. All six i.n. immunized hamsters infected with the virus exhibited much less body-weight loss. They had a lower level of live virus detection in their throat swabs (Fig. 6f, group 2) than the infected naive hamsters (Fig. 6f, group 1), verifying again that the i.n. immunizations with the S-Fc induced protective immunity at viral entry sites. In the exposed animals, four of the six naive unimmunized hamsters exposed to the i.n. immunized, SARS-CoV-2-infected hamsters had no detectable live virus during the 10 days (Fig. 6f, group 2). Similarly, four of the six i.n. immunized hamsters exposed to SARS-CoV-2-infected naive unimmunized hamsters had no live virus detectable during the 10 days (Fig. 6f, group 3). However, the live virus was detected in two of the i.n. immunized hamsters, the virus titers were significantly lower (Fig. 6f, group 3). In contrast, all six naive unimmunized hamsters exposed to the virally infected hamsters that were i.m. immunized with the S-Fc protein displayed a high titer of live SARS-CoV-2 virus in their throats (Fig. 6f, group 4). However, the virus detection was delayed 2–3 days, suggesting that i.m. immunized animals can spread the virus. In addition, all six i.m. immunized hamsters exposed to SARS-CoV-2-infected naive unimmunized hamsters had live viruses detected in their throats during the 10 days (Fig. 6f, group 5), indicating they all failed to prevent viral transmission. Viral load was also quantified as SARS-CoV-2 N gene RNA in throat swab fluid on 1–4 dpe (days post-exposure). The results from the N RNA detection were consistent with the results of the live-virus detection (Fig. S8b–f). Together, our study unambiguously demonstrates that the i.n. immunization by the S-Fc protects hamsters by decreasing viral shedding and preventing airborne SARS-CoV-2 transmission (Table S1).

Discussion

This study explores a respiratory vaccination strategy by using the mucosa-specific, FcRn-mediated IgG Ab transfer pathway to reduce or eliminate SARS-CoV-2 replication and spread in or through the nose and lungs. The present study produced several lines of evidence. First, the S-Fc-immunized mice had higher IgG and IgA Abs in nasal washes, BAL, and blood compared with those immunized by S alone or FcRn KO mice immunized by S-Fc. Also, the S-Fc-immunized mice exhibited more potent nAb activity than the control animals. Second, as opposed to the PBS control animals, hamsters or hACE2-transgenic mice i.n. immunized by S-Fc developed resistance to the ancestral SARS-CoV-2 infection, exhibiting reduced virus replication in the nasal turbinate, lung, and mouse brain. We detected high levels of live virus in the brains of the infected unimmunized hACE2 mice but not in the infected hamsters. The expression level and localization of human ACE2 in transgenic animals may explain this discrepancy. For example, hamsters expressing human ACE2 also have high virus titers detected in the

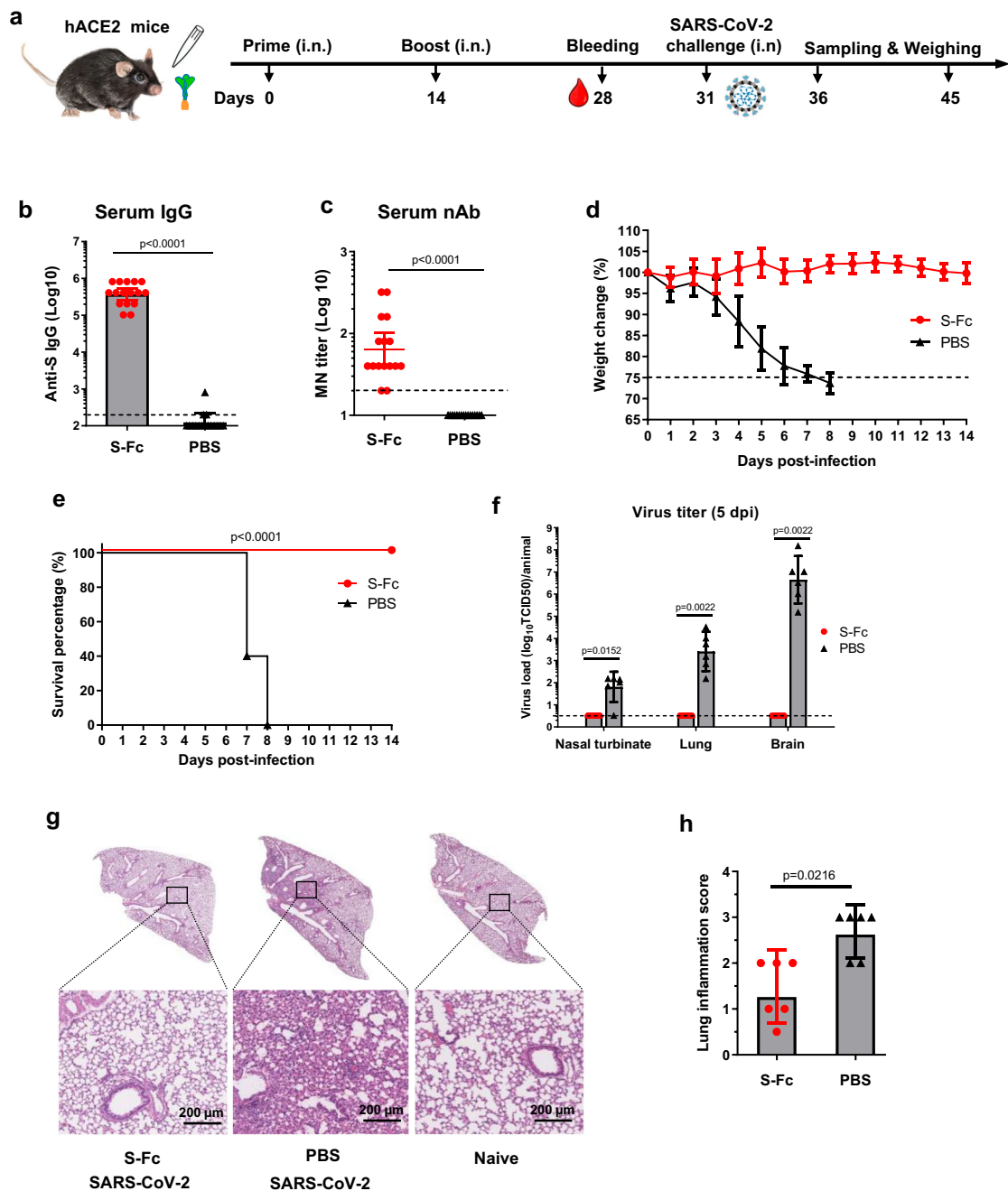
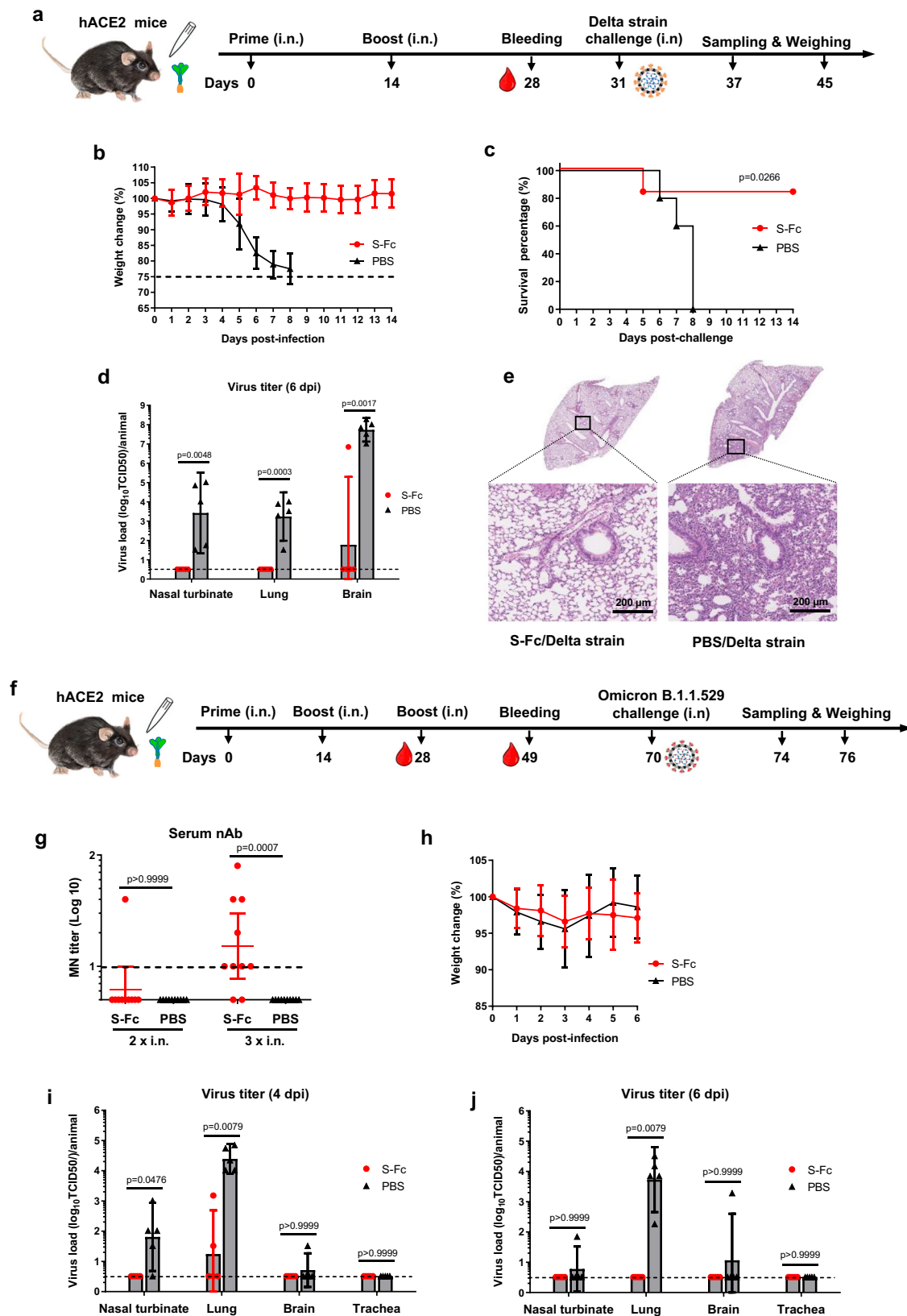


Fig. 3 | Intranasal immunization by the S-Fc induces protective immunity to intranasal (i.n.) challenge with ancestral SARS-CoV-2. a Ten μg of S-Fc or PBS with 10 μg CpG was i.n. administered into 8-week-old hACE2 mice ($n = 16$ per group). Mice were boosted 14 days after primary immunization. Six mice in each group were euthanized at 5 days post-infection (dpi) for sampling and virus titration. The remaining 10 mice in each group are subjected to the body weight loss and survival analysis. **b, c** Serum anti-S-specific IgG Ab titers (**b**) and neutralizing Ab (**c**) in hACE2 mice ($n = 16$ per group). The S-specific IgG Ab titers were measured by coating ELISA plates with S protein; the micro-neutralization test determined the neutralizing Ab activity in the immunized sera. The data represent a geometric mean with 95% CI. **d** Body weight changes following the challenge. Seventeen days after the boost, groups of mice (S-Fc group, $n = 10$; PBS group, $n = 10$) were i.n. challenged with the ancestral SARS-CoV-2 (2.5×10^4 TCID₅₀) and weighed daily for 14 days. Mice were humanely euthanized at the end of the experiment or when a humane endpoint was reached. The data represent the mean \pm SD. **e** Survival

following virus challenge ($n = 10$ per group). The percentage of mice protected was shown by the Kaplan–Meier survival curve. **f** Viral titers in the nasal turbinates, lung, and brain at 5 dpi. The virus titers in the samples of the immunized and control mice ($n = 6$) were determined by CPE in Vero E6 cells cultured for 4 days. The viral titers were shown as TCID₅₀ from each animal sample. The data represent a geometric mean with 95% CI. **g** Histopathology of the lungs from the challenged mice ($n = 6$ per group). Lungs were collected at 5 dpi. The lungs from uninfected mice were included as standard control ($n = 6$). The lung sections were stained with Hematoxylin-Eosin (H & E). The representative slides are shown. All scale bars represent 200 μm. **h** The inflammatory responses of each lung section ($n = 6$ per group) were scored blindly and shown as geometric mean with 95% CI. The statistical analyses were performed by Mann–Whitney test (two-tailed) (**b, c, f, h**) and Log-rank (Mantel-Cox) test (**e**). Dash lines indicate LOD or humane endpoint (**d**). Source data are provided as a Source data file.



brain following exposure to SARS-CoV-2²⁵. Third, the S-Fc-immunized, hACE2 mice effectively protected against infections by the SARS-CoV-2 Delta or Omicron B.1.1.529 variants. An additional booster was required to protect hACE2 mice from Omicron infection completely. Likewise, to induce broad nAbs against the Omicron strain, it is evident that two boosters are also required for the mRNA vaccinations²⁶. However, this

is not surprising because Omicron variants possess more mutations in its S protein and are shown to be resistant to immune responses elicited by the S protein from the ancestral strain. We conducted a test to assess the efficacy of sera obtained from immunized mice and hamsters in neutralizing different strains of SARS-CoV-2 (Fig. S11a-f, Supplementary note 4). Our findings indicate that, while the sera from

Fig. 4 | Intranasal immunization by the S-Fc induces protective immunity to intranasal challenge with SARS-CoV-2 Delta or Omicron variants. **a** The 8-week-old hACE-2 mice ($n = 10$ – 11) were i.n. immunized by $10 \mu\text{g}$ S-Fc or PBS with $10 \mu\text{g}$ CpG and boosted 14 days later. **b** Seventeen days after the boost, S-Fc ($n = 11$) and PBS ($n = 10$) groups were i.n. challenged with Delta strain (2.5×10^4 TCID₅₀). Six mice in S-Fc group and 5 mice in PBS group were subjected to the body weight loss and survival analysis by the Kaplan–Meier survival curve (**c**). The remaining five mice in each group were euthanized at 6 dpi for sampling the nasal turbinate, lung, and brain and measuring the Delta virus titers by TCID₅₀ (**d**). **e** Lungs ($n = 5$ per group) were collected at 6 dpi. The lung sections were stained with Hematoxylin-Eosin (H & E). A representative lung image from 5 lungs was shown. **f** The 8-week-old hACE-2 mice were i.n. immunized by $10 \mu\text{g}$ S-Fc ($n = 10$) or PBS ($n = 10$) with $10 \mu\text{g}$ CpG and boosted 14 and 28 days later, respectively. Mice were i.n. challenged with the

Omicron B.1.1.529 (1×10^6 TCID₅₀) 42 days after the boost. **g** Two weeks after the first or 3 weeks after the second boost, sera from 10 mice per group were measured for the neutralizing Ab titers. **h** Groups of 10 mice were weighed daily for 4 or 6 days after the challenge. **i, j** The Omicron B.1.1.529 virus titers were determined at 4 or 6 dpi in the nasal turbinate, lung, and brain of the S-Fc immunized and control mice ($n = 5$). Supernatants of the tissue homogenates were added to VAT cells and incubated for 4 days; the viral titers were shown as TCID₅₀. The body weight data in (**b**) and (**h**) were shown as mean \pm SD, while the data in **d, g, i, j** represent a geometric mean with 95% CI. The Mann–Whitney test (two-tailed) was used for the statistical assays (**d, g, i, j**), while the Log-rank (Mantel-Cox) test was used for the survival analysis (**c**). Dashed lines represent LOD. Source data are provided as a Source data file.

immunized animals could effectively neutralize SARS-CoV-2 strains α , β , γ , δ , ϵ , they were found to be ineffective against Omicron strains BA.5 or XBB.1.5. Similarly, studies have shown that the sera from people who received an ancestral SARS-CoV-2 mRNA vaccine booster were unable to effectively neutralize Omicron strains BA.2.12.1, BA.4, BA.5²⁷, or an ancestral SARS-CoV-2/BA.5 bivalent mRNA vaccine was unable to induce neutralizing antibodies against Omicron strains BQ.1, BQ.1.1, XBB, and XBB.1²⁸. As a result, it is critical to update the Spike antigen to reflect predominant Omicron strains and develop antibodies against these variants. To ensure the efficacy of our S-Fc antigen against the latest Omicron strains, we updated it using the Spike from XBB.1.5. Our utmost objective is to create a nasal vaccine that can actively elicit broad-spectrum protective immune responses against various SARS-CoV-2 variants. Fourth, remarkably, most S-Fc-immunized animals exhibited significantly reduced inflammation in the lungs of hACE2 mice.

In the airborne transmission study, in striking contrast to the unimmunized hamsters or hamsters immunized by the i.m. route, most i.n. S-Fc immunized hamsters infected with the virus did not spread the virus to unimmunized hamsters. Similarly, most i.n. S-Fc immunized hamsters were not infected when placed with the infected unimmunized hamsters. An incomplete block of transmission by intranasal immunization may result from high virus doses during donor hamster infection and extended housing periods for infected and exposed animals. It would be interesting to know if hamsters received i.n. S-Fc immunization could prevent the spread of Omicron subvariants. Unfortunately, the low efficiency of airborne transmission of Omicron BA.1, BA.2.12.2, BA.5²⁹, and XBB.1.5 (Fig. S9) in hamsters makes it challenging to evaluate our nasal vaccines in blocking Omicron airborne transmission. However, Omicron variants can also be transmitted via fomites^{29,30} and a COVID-19 nasal vaccine should protect against airborne and fomite transmission. Therefore, it is pertinent to examine whether intranasal immunization with the XBB.1.5 derived S-Fc protein can effectively protect against fomite transmission of Omicron variants like XBB.1.5, Eg.5, and BA.2.86. This question merits further investigation.

Several mechanisms may account for protection against SARS-CoV-2 infection and transmission. FcRn binds S-Fc in acidic pH conditions. A slightly acidic pH in the respiratory tract³¹ is expected to facilitate FcRn to retain antigens in airway mucosal surfaces and transfer them across the airway barrier, as shown by our previous studies^{32,33}, and others³⁴. The local Ab immune responses can represent a primary barrier of immune defense against viral infections of the respiratory tract, characterized by the presence of sIgA in the nasal mucosa or IgG in the BAL¹⁰. The natural SARS-CoV-2 infection induces mucosal sIgA, which dominates the early nAb response to SARS-CoV-2 with potent neutralizing activity^{5,35}. Furthermore, the levels of mucosal Abs determine the viral load and the time required to recover from systemic symptoms. In this study, the mice and hamsters that were i.n. immunized by S-Fc developed high levels of IgA Abs in the nasal washes and BAL. These results are consistent with the findings of

previous studies where FcRn-targeted respiratory immunizations against viral mucosal infections^{9,32,33} and adenovirus-vectored SARS-CoV-2 nasal vaccine^{36,37} elicit high Ab responses. In addition, the mice or hamsters i.m. immunized by S-Fc failed to produce significantly increased levels of IgA Abs in the nasal washes, despite high IgG Abs in the BAL. A robust SARS-CoV-2 infection in nasal turbinates is readily detectable after the adoptive transfer of the nAbs³⁸. This observation is further supported by our findings that hACE2 mice succumb to nasal infection following an adoptive transfer of serum Abs from i.n. immunized mice by S-Fc (Fig. S12). It's possible that passive Ab transfer may not protect hACE2 mice from SARS-CoV-2 infection because the Abs may not be able to pass through the blood-endothelial barrier and reach the olfactory mucosa³⁹. Indeed, i.m. vaccination fails to reduce viral load in nasal swabs or turbinate significantly⁴⁰. Considering SARS-CoV-2 also infects cells via a cell-to-cell fashion⁴¹, it may be difficult for serum IgG Abs to block viral entry and spread in the upper respiratory tract, or a high level of IgG Abs is required. In addition, we found high levels of S2-specific IgG Abs in the immunized mice (Fig. S11g). It's important to note that S2 is more conserved across different versions of SARS-CoV-2, so although we don't show the protective functions of S2-specific Abs, they are expected to play a significant role in defending against the virus. FcγR-dependent Ab effector functions are crucial for achieving vaccine-mediated protection⁴².

FcRn-mediated respiratory delivery of vaccine antigen facilitates the production of memory immune responses. The induction of S-specific memory immune responses is crucial for a vaccine to provide sustained protection⁴³. The S- or RBD-specific nasal Abs can last 9 months in COVID-19 patients⁴⁴. FcRn-mediated respiratory vaccination with S-Fc induces and sustains high levels of S-specific IgA and IgG and plasma cells 8 months after the boost, which they resist lethal SARS-CoV-2 infection at least 6 months after the boost. TRM T cells in the lung can promote rapid viral clearance at the site of infection and mediate survival against lethal viral infections, especially in severe COVID-19 patients^{17,45}. Our study demonstrated that a higher percentage of CD4⁺ or CD8⁺ TRM T cells were present in the lungs of mice that received i.n. S-Fc immunization than in those of PBS control animals. Furthermore, the i.n. immunization induced significantly more lung-resident TRM cells than the i.m. route. This is consistent with previous findings by directly delivering viral antigens into the airway^{9,17}. Additionally, FcRn prolongs IgG half-life^{14,15}. Thus, FcRn binding to S-Fc is expected to stabilize S-Fc in vivo, enhancing FcγRs-mediated uptake of S-Fc by antigen-presenting cells^{46,47}. Likely, TRM T cells are particularly critical against the SARS-CoV-2 variants that undergo rapid mutations and evade antibody immunity. Further studies are needed to demonstrate how long these TRM T and B cells^{16,48} may persist in the lung and how they contribute toward long-term protection against the SARS-CoV-2 variants. SARS-CoV-2-specific CD8⁺ TRM cells are detectable for at least two months after viral clearance in the nasal mucosa⁴⁵.

Several rationales could explain the rise in breakthrough infections, two of which are most likely. First, i.m. vaccination couldn't effectively induce local immunity in the respiratory mucosa. Indeed,

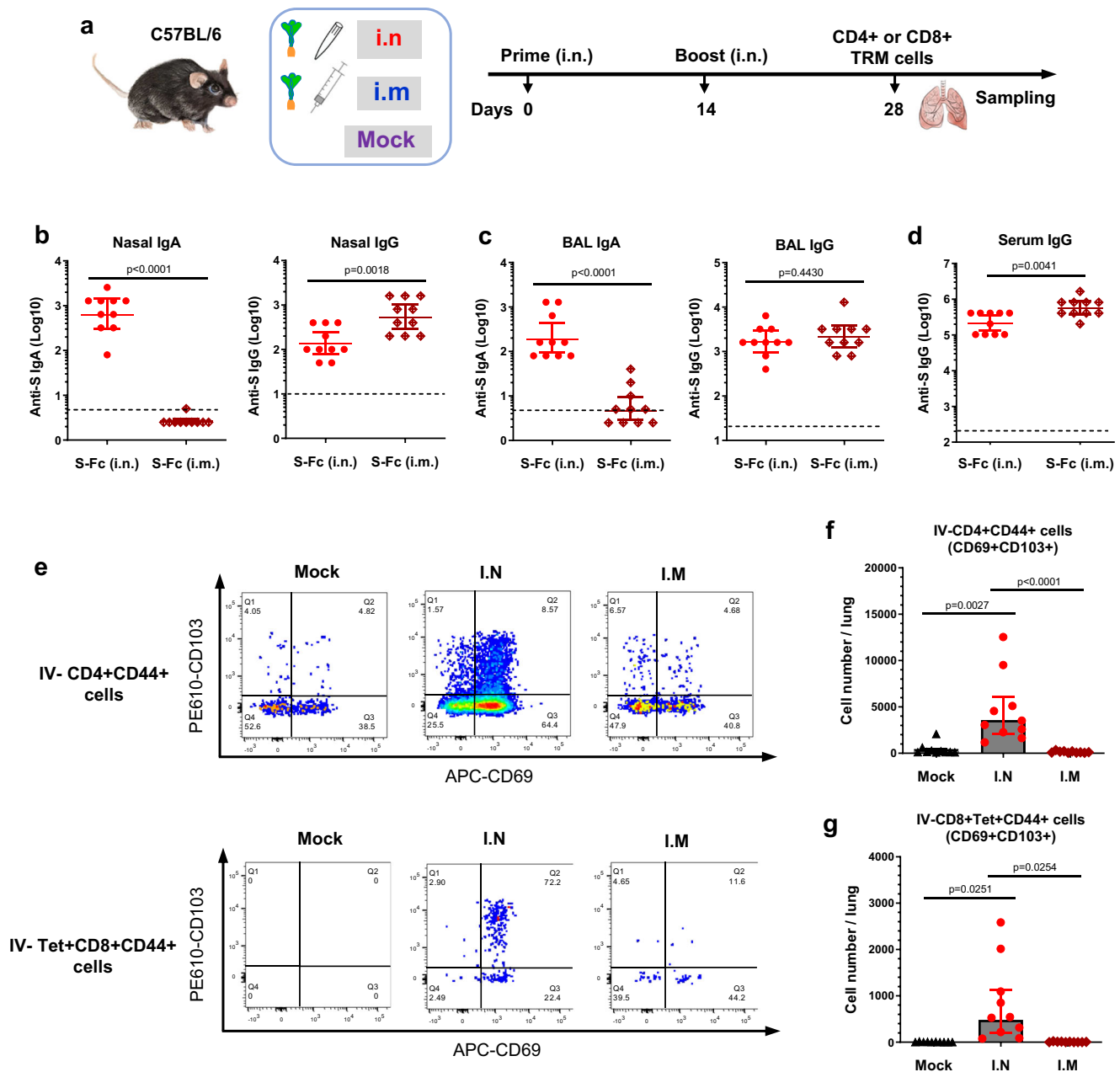
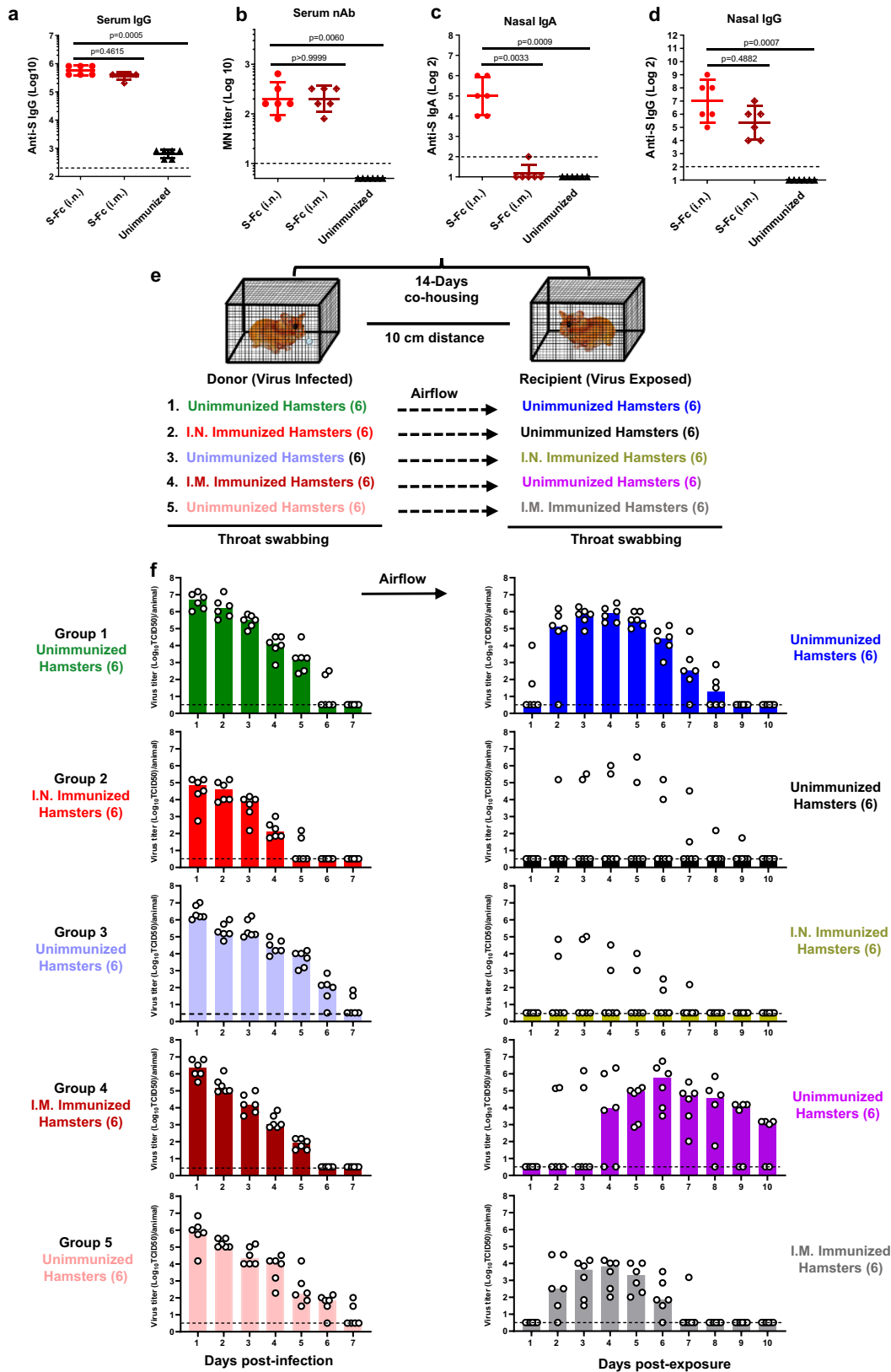


Fig. 5 | FcRn-mediated intranasal vaccination significantly induces S-specific local immune responses in the respiratory tract. A Ten μg of S-Fc or PBS in combination with 10 μg of CpG was i.n. administered into 6–8-week-old mice ($n = 10$). Mice were boosted 14 days after primary immunization. An additional group of mice ($n = 10$) that were intramuscularly (i.m.) immunized in 10 μg S-Fc with 10 μg of CpG was included as an i.m. route control. Tissues and blood were collected at the indicated time points. **b–d** Anti-SARS-CoV-2 S-specific IgA or IgG Ab titers in nasal washings (**b**), BAL (**c**), and serum (**d**) after the boost. S-specific Abs was measured by ELISA 14 days after the boost in 10 representative mouse samples per group. The data represent a geometric mean with 95% CI. **e–g** Tissue-resident memory (TRM) T cells in mouse lungs. The IV-CD4⁺CD44⁺CD69⁺CD103⁺ or IV-CD8⁺Tet⁺CD44⁺CD69⁺CD103⁺ TRM T cells in the lungs were assessed 14 days after

the boost by FACS. Flow cytometry plots represent results from two independent experiments with 5 individual samples per group. Numbers in the top right quadrants (**e**) or the graph (**f**, **g**) indicate the percentage or number of TRM CD4⁺ or CD8⁺ T lymphocytes following i.n. or i.m. immunizations. The data in (**f**) and (**g**) represent a geometric mean with 95% CI. The unpaired t-test (two-tailed) was used for the statistical analysis of data from experiment (**b**) (Nasal IgG) and (**c**). The Mann–Whitney test (two-tailed) was used for experiment (**b**) (Nasal IgA) and (**d**). One-way ANOVA (Kruskal–Wallis test followed by Dunn’s multiple comparisons tests) was used for analyzing the results of experiment (**f**), while the Welch’s ANOVA test (with Dunnett’s T3 multiple comparisons test) was used for experiment (**g**). Dashed lines denote LOD. Source data are provided as a Source data file.

the i.n., but not i.m., immunizations with S-Fc induce nasal IgA and TRM T cells in the lung. Second, individuals infected by SARS-CoV-2 through the nasal epithelial cells can asymptotically shed the infectious virus for an unknown time. Hence, we envision the nasal vaccination as an essential complementary strategy to the i.m. vaccines that are authorized or undergoing clinical trials. Because FcRn can transfer the immune complexes across the mucosal epithelial

barrier with or without pre-existing Abs^{13,49}, we do not expect that the efficacy of the FcRn-targeted mucosal vaccination is influenced by pre-existing SARS-CoV-2 immunity. An instance of the S-Fc i.n. immunization of hamsters previously infected by Omicron B.1.1.529 resulted in a significant enhancement of pre-existing serum IgG levels, along with increased levels of both nasal IgA and IgG (Fig. S10). The FcRn-mediated nasal vaccine can be used as the first dose for an



unimmunized person or booster for those who have been immunized, even previously infected by SARS-CoV-2. The combination of mucosal and parenteral vaccines has been proven effective at mucosal entry against SARS-CoV-2 infections^{7,9,50,51}.

In addition to pneumonia and acute respiratory distress, some symptomatic or asymptomatic COVID-19 patients, including those

with breakthrough infections, are reported to experience a long COVID^{52,53}. The exact causes of the long COVID are elusive; they may involve direct effects of viral infection or indirect influences on the brain. In humans, the nasal olfactory epithelium expresses a high level of ACE2 receptor. Although debatable, SARS-CoV-2 may enter the brain by crossing the neural-mucosal interface in olfactory mucosa⁵³ or

Fig. 6 | Intranasal immunizations with the S-Fc protein reduce virus transmission from vaccinated to unvaccinated hamsters or vice versa. **a–d** Groups of male hamsters ($n = 6$) were i.n. or i.m. immunized with 30 μg of S-Fc and 30 μg of CpG twice in a 2-week interval. The unimmunized hamsters were used as a negative control. Anti-ancestral SARS-CoV-2 strain S-specific IgA, IgG Ab, and neutralizing Ab titers in sera and nasal washings were measured by ELISA 14 days after the boost. The data represent a geometric mean with 95% CI. The statistical analyses in **a–d** were conducted by one-way ANOVA (Kruskal–Wallis test followed by Dunn’s multiple comparisons tests). Dashed lines indicate LOD. **e** A schematic illustration of the experimental design. Briefly, 5 groups of hamsters are included, and each group has 6 hamsters for virus donors and 6 hamsters for virus recipients. The

donor hamsters were unimmunized or immunized with S-Fc plus CpG via i.n or i.m. routes. Then the donor hamsters were infected with 1×10^5 TCID₅₀ ancestral SARS-CoV-2 strain. Fourteen hours later, donor hamsters in the wire cages were separately cohoused with 6 unimmunized or immunized hamsters within the same isolator. Throat swabbing was performed for 7 days for donor hamsters (1–7 dpi) and 10 days for recipient hamsters (1–10 days post-exposure). **f** Virus loads in the throat swabs from the donor and recipient hamsters. The infectious live virus in the samples was measured in VAT cells for 4 days of culture. The viral titers were shown as TCID₅₀ from each animal sample. Each open circle represents one animal, and the bar indicates the median value of each group at the indicated time points. Source data are provided as a Source data file.

infecting the olfactory epithelium or bulb, or both⁵⁴. Indeed, SARS-CoV-2 is identified to replicate in brain astrocytes⁵⁵. Alternatively, inflammatory cytokines derived from inflamed lungs or other organs may cross the blood-brain barrier⁵⁶. Consequently, a virus or cytokine may cause encephalitis or necrosis, leading to a long COVID. The hACE2 mice are highly susceptible to SARS-CoV-2 infection with the virus detected in the brain²⁰. Our study confirms this and shows that FcRn-mediated respiratory vaccination can prevent brain viral infection in hACE2 mice. Likely, the sIgA or TRM T cells induced by S-Fc can efficiently block the viral replication in nasal turbinates, reducing viral infection in the olfactory epithelium or access to the olfactory bulb.

We developed a respiratory vaccine using pre-stabilized SARS-CoV-2 S antigen that stimulates local and systemic protective immunity. According to our model (Fig. S13), mucosal antigen-presenting cells that express FcγR, like dendritic cells, absorb the S-Fc protein that is transported across respiratory epithelial cell monolayer by FcRn and then migrate to mediastinal draining lymph nodes where they activate CD4⁺ T cells and trigger the B cell response in the germinal centers. By increasing the persistence of the S-Fc in tissue and circulation, the vaccination may further enhance the development of long-term humoral and cellular immunity. The substantially longer half-life of IgG in humans compared to mice or hamsters (21 vs. 6 days) would ensure high and persisting levels of S-Fc in human immunization. Also, the S-Fc and human IgG1 had a lower affinity to the mouse FcγRI, but it exhibits a high affinity with human FcγRI (Fig. 1d), suggesting our S-Fc vaccine may work more efficiently in humans. Although the i.n. administered viral vaccines induce protection in the respiratory tracts^{36,37,40}, a protein-based nasal vaccine may be preferred, especially in young, elderly, and immunocompromised populations. It is also interesting to compare the protective immunity in the upper respiratory tract and protection against infection and transmission induced by our protein-based nasal vaccine and the licensed mRNA vaccine. Together, our results indicate that FcRn-mediated respiratory immunization can be an effective and safe strategy for maximizing the efficacy of vaccinations against infection and transmission of SARS-CoV-2 and its emerging variants.

Methods

Mice and Golden Syrian hamsters

All research experiments in this study comply with all relevant ethical regulations. The Institutional Animal Care and Use Committee approved the animal protocol at the University of Maryland (#R-APR-20-18 and #R-MAR-21-19). The animals were acclimatized at the animal facility for 4–6 days before initiating experiments. Animals from different litters were randomly assigned to experimental groups, and investigators were not blinded to allocation during experiments and outcome assessment. Wild-type (WT) C57BL/6 mice were purchased from Charles River Laboratories (Frederick, MD), and FcRn KO mice were a gift from Dr. Derry Roopenian (Jackson Laboratory, Bar Harbor, ME). Transgenic mice expressing human ACE2 by the human cytokeratin 18 promoter (K18-hACE2) represent a susceptible rodent model^{20,57}. Specific-pathogen-free, 6–8-week-old, female and male

B6.Cg-Tg(K18-ACE2)2Prlmn/J (Stock No: 034860, K18-hACE2) hemizygous C57BL/6 mice and control C57BL6 mice (non-carriers) were purchased from the Jackson Laboratory and used for breeding pairs to generate pups for research. All the offspring were subjected to genotyping, and only the hemizygous K18-hACE2 mice were chosen for future use. Seven-week-old male/female Golden Syrian hamsters were obtained from Charles River Laboratories. Animals have been maintained in individually ventilated cages at ABSL-2 for noninfectious studies or in isolators within the ABSL-3 facility for studies involving SARS-CoV-2 viruses. Immunization and virus inoculation were performed under anesthesia. We avoided using volatile chemical anesthetics known to increase the permeability of the respiratory epithelial barrier in nasal immunizations. All mice were anesthetized with an intraperitoneal (i.p.) injection of fresh Avertin at 10–12.5 μl of working solution (40 mg/ml) per gram of body weight and laid down in a dorsal recumbent position to allow for recovery. Hamsters were sedated with Dexmedetomidine (50–250 $\mu\text{g}/\text{kg}$) via subcutaneous injection for immunization and virus infection, or they were anesthetized with isoflurane for collecting blood, nasal washes, and throat swabs.

Cells, antibodies, and viruses

Vero E6 (with high expression of endogenous ACE2, Cat No. NR-53726) and VAT (Vero E6-TMPRSS2-T2A-ACE2, Cat No. NR-54970) were from Biodefense and Emerging Infections Research Resources Repository (BEI Resources, Manassas, VA). Chinese hamster ovary (CHO) cells were purchased from the American Tissue Culture Collection (ATCC, Manassas, VA). Vero E6, VAT, and CHO cells were maintained in complete Dulbecco’s Minimal Essential Medium (DMEM) (Invitrogen Life Technologies), supplemented with 10% fetal bovine serum (FBS), 2 mM L-glutamine, nonessential amino acids, and antibiotic and antifungal (100 units/ml of penicillin, 100 $\mu\text{g}/\text{ml}$ of streptomycin, and 250 ng/ml of amphotericin B). Vero E6, VAT, and CHO cells routinely tested negative for Mycoplasma sp. by real-time PCR. Recombinant CHO cells were grown in a complete medium with G418 (Invitrogen, 1 mg/ml). All cells were grown at 37 °C in 5% CO₂.

The insect cell-expressed SARS-CoV-2 Spike S2 (Cat # NR-53799), S-specific mAbs 2TP1B11, 2TP2C7, and 2TP2E7 were procured from the BEI Resources. S-specific mAbs 40150-R007, 40952-MM57, and SPD-M128, as well as anti-S polyclonal antibodies 40590-T62 and 40150-T62-Cov2, were acquired from Sino Biologicals. Hamster IgG2 was purchased from BD (Cat # 553294). Motavizumab, an antibody against the respiratory syncytial virus (RSV) F protein, was acquired from Cambridge Biologics (Brookline, MA). The sera from the convalescent COVID-19 patients or health persons were a gift from the Biotech Laboratories (Rockville, MD). The horseradish peroxidase (HRP)-conjugated anti-human IgG (Cat# 2081-05), anti-goat IgG (Cat# 6160-05), streptavidin (Cat# 7100-05), and biotin-labeled goat anti-mouse IgA (Cat# 1040-08) were obtained from Southern Biotech (Birmingham, AL). HRP-conjugated anti-mouse IgG Fab (Cat# A9917) and anti-human IgG Fab (Cat# SAB4200791) were from Sigma. HRP-conjugated anti-mouse IgG (Cat# PA1-28568) and anti-hamster IgA

48 hrs, loaded onto an anti-His resin column, and eluted with 0.1M glycines (pH 2.5). The eluted proteins were neutralized with 1M Tris-HCl (pH 8.0), and the protein buffer was replaced with PBS using Amicon Ultra-15 Centrifugal Filter Unit (10 K). The purified proteins were visualized by SDS-PAGE and Coomassie staining. The site-specific biotinylation was then conducted by using a BirA biotin-protein ligase standard reaction kit (Cat# BirA500) from Avidity Biosciences (Aurora, CO).

SDS-PAGE gel and Western blotting

Protein quality was assessed by 8–15% SDS-PAGE gel under reducing conditions. Proteins in gels were either stained with Coomassie blue dye in gel or used for transfer onto nitrocellulose membranes (GE Healthcare). The membranes were blocked with 5% milk in PBST (PBS and 0.05% Tween-20) and incubated with appropriate primary and HRP-conjugated secondary antibodies, as indicated in the Figure legends. The immobilized Western chemiluminescent HRP substrate (Millipore, Cat# WBKLS0100) was used to visualize protein bands in membranes and images captured by the Chemi Doc XRS system (BioRad).

Samplings of nasal washes, bronchoalveolar lavage, and throat swabs

The nasal washes and BAL fluids were collected from the mouse under euthanasia with over-dosage of Avertin. For sampling nasal washes, we removed the lower jaw. A small incision was made over the ventral aspect of the trachea; then, a syringe with a blunt plastic tip was inserted into the trachea toward the nasal cavity. 1 ml PBS was gently injected into the nasopharynx and collected when it flowed from the external nares. For BAL collection, the syringe was inserted into the trachea but toward the lungs, and 1 ml of PBS was carefully injected into the lungs by keeping the syringe in position. The PBS was retrieved back to obtain BAL fluids. The nasal washes and BAL fluids were centrifuged to remove cellular debris, concentrated to 350 μ l with Amicon 0.5 ml centrifugal filter unit (10 K) (Millipore, Cat# UFC501096), and the supernatants were stored at -20°C .

To collect nasal washes in hamsters, animals were anesthetized with isoflurane, and small-sized feeding needles (20 G) were used to inject 500 μ l sterile PBS into the nostrils (250 μ l each side). The outflows were collected in a petri dish as expelled by the hamster. The volume was increased to 0.5 ml with the addition of cold PBS. To collect throat swabs from the anesthetized hamsters, the swab was first moistened in 650 μ l DMEM media with 1% inactivated FBS and then placed into the throat, where it was gently rubbed around ten times. These swabs were then soaked for 5 minutes in the vials containing the remainder of the media. Subsequently, the throat swabs were removed, and the samples were vortexed and stored at -80°C for further virological analysis.

Enzyme-linked immunosorbent assay (ELISA) or spot (ELISpot)

IgA and IgG antibodies in nasal washes, BAL fluid, and sera reactive to SARS-CoV-2 spike antigens were quantified by ELISA as previously described^{9,32,33}. In brief, 96-well plates (Maxisorp, Nunc) were coated with 1 μ g/ml of the S protein described above in 100 μ l coating buffer (PBS, pH 7.4) per well and incubated overnight at 4°C . Plates were washed four times with 0.05% Tween 20 in PBS (PBST) and blocked with blocking buffer (2% bovine serum albumin in PBST) for 2 h at room temperature. Sera were heat-inactivated at 56°C for 30 min before serial dilutions starting at 1:200 in dilution buffer. The serially diluted specimens (nasal wash, BAL, or sera) from animals were added to each well and incubated for 2 hrs. After washing six times with PBST, the detection antibodies were added and incubated for 1.5 hr at room temperature. HRP-conjugated rabbit anti-mouse IgG (1:20,000, Invitrogen, Cat# PA1-28568) was used for measuring mouse IgG, while biotin-labeled goat anti-mouse IgA Ab (1:5000, Southern Biotech,

Cat#1040-08) plus HRP-conjugated streptavidin (1:7000, Southern Biotech, Cat# 7100-05) were used for measuring mouse IgA antibody. To detect S-specific hamster IgG, goat anti-hamster IgG (1:4000, Novus, Cat# NB1207141) plus HRP-conjugated rabbit anti-goat IgG (1:5000, Southern Biotech, Cat# 61-6065) were used. To determine S-specific hamster IgA, HRP-conjugated anti-hamster IgA (1:250, Brookwood Biomedical, Cat# sab3003a) was used. One hundred microliter TMB (tetramethylbenzidine) (BD, Cat# 555214) was used as a substrate to visualize the signals. The reactions were stopped after 5 min by adding 100 μ l of 1 M sulfuric acid before reading on a Victor III microplate reader (Perkin Elmer) at OD450 nm. Antibody endpoint titers were determined by non-linear regression as the reciprocal of the highest sample dilution with an absorbance above two times the absorbance of blank wells.

For measuring S-specific antibody-secreting cells (ASCs) in bone marrow, an ELISpot kit (MabTech, Cat# 3825-2H) was used. The 96-well ELISpot plates (MabTech, Cat# 3654-TP-10) were pre-wetted with 35% ethanol and washed five times with sterile water plus 1 with PBS. The plates were then coated with S protein at 20 μ g/ml overnight at 4°C (100 μ l/well) and blocked with RPMI 1640 complete medium with 10% FBS for 2 h at room temperature. Bone marrow cells from femurs and tibias were collected in RPMI 1640, filtered through a 70 μ m strainer, and subjected to ACK lysis. Serial dilutions of single-cell suspensions were prepared in RPMI 1640 and added to the coated wells for 18–24 h at 37°C in 5% CO_2 . After incubation, the plates were emptied and washed five times with PBS, then incubated with biotinylated anti-mouse IgG (0.5 μ g/ml) for 2 h at room temperature. After washing with PBS, HRP-streptavidin (1:700) was added and incubated for 1 h. The samples were developed with TMB substrate until distinct spots emerged. After washing, the plates were stored upside down in the dark to dry overnight at room temperature. Spots were counted with an ELISpot reader (AID, Germany).

Characterization of the S-Fc or S proteins

The ELISA assays were also used to measure interactions of the S-Fc or S with (1) human, mouse, or hamster FcRn/ β 2m heterodimer (ACRO-Biosystems, Cat# FCM-H82W4 for human FcRn/ β 2m; Cat # FCM-M82W6 for mouse FcRn/ β 2m; at the acidic pH (6.0) and neutral pH (7.4) conditions; (2) human, mouse, or hamster Fc γ RI (ACROBiosystems, Cat# FCA-H82E8 for human Fc γ RI; Cat# CD4-M82E7 for mouse Fc γ RI); (3) human ACE2 (ACROBiosystems, Cat# AC2-H82E6); and (4) human and mouse C1q protein (Complement Technology, Cat#A099, and #M099). All FcRn/ β 2M heterodimer, Fc γ RI, ACE2, and C1q proteins were conjugated with biotin to facilitate detection. In brief, ELISA plates were coated with S-Fc or S protein in PBS (1 μ g/well for FcRn/ β 2M binding or 200 ng/well for Fc γ RI and hACE2 binding) overnight at 4°C . After blocking for 2 h, the 2-fold serial diluted target proteins (4–4000 ng/ml of FcRn/ β 2m, 0.4–400 ng/ml of Fc γ RI and hACE2) were added and incubated for 2 h at room temperature. For the C1q binding assay, S-Fc or S proteins were used to coat plates at a serial dilution (800–7.8 ng/well), and a biotin-conjugated human or mouse C1q (2 μ g/ml) was used for detection. For all assays, the streptavidin-HRP was from Southern Biotech (1:5000), and TMB was used to visualize the colorimetric signals. The Victor III microplate reader read the plates at 450 nm to assess optical density (OD).

Quantification of SARS-CoV-2 virus and RNA

The number of infectious virus particles in the specimen of ancestral SARS-CoV-2 or Delta strain infected animals was determined in Vero E6 cells by 50% tissue culture infectious dose (TCID_{50}) endpoint dilution assay as described⁶². The quantification of the Omicron strain was performed in VAT cells. To increase the sensitivity, VAT cells were also used in detecting ancestral viruses and Omicron variants in the throat swab samples, as the overexpression of the hACE2 and TMPRSS2 in VAT cells enhances the replication efficiency of the SARS-CoV-2⁶³.

Briefly, cells were plated at 15,000 cells/well in DMEM with 10% FBS and incubated overnight at 37 °C with 5.0% CO₂. Media was aspirated and replaced with DMEM with 1% inactivated FBS for virus infection. Animal tissues, including nasal turbinate, lung, brain, intestine, and kidney, were homogenized in the TissueLyser LT (Qiagen). After centrifuging at high speed (18407 × g, 10 min), the 10-fold serial dilutions of supernatants were used to infect the cell monolayers in 96-well plates, and the CPE was checked after 4 days. Positive (virus stock of known infectious titer) and negative (medium only) controls were included in each assay. The virus titer was expressed as TCID₅₀/ml (50% infectious dose (ID₅₀) per milliliter) by using the Reed-Muench method⁶².

To monitor viral RNA levels in virus-infected animal samples (throat swabs), total RNAs were isolated by using the PureLink RNA mini kit (Invitrogen, Cat# 12183018A) and subjected to the one-step quantitative real-time reverse transcription-PCR assay (qRT-PCR) using TaqMan Fast Virus 1-Step Master Mix (ThermoFisher, Cat# 4444432) as described previously^{64,65}. A SARS-CoV-2 nucleocapsid (N) specific primers and probe sets were used: Forward primer: 5'-GACCCCAAAAT-CAGCGAAAT-3'; Reverse primer: 5'-TCTGGTACTGCCAGTTG AATCTG-3'; and probe: 5'-FAM-ACCCCGCATTACGTTTGGTGACC-BHQ1-3'. Briefly, viral RNA was expressed as N gene RNA copy numbers from each swab or animal, based on an RNA standard included in the assay, which was created via the *in vitro* T7-DNA-dependent RNA transcription of a linearized DNA molecule containing the target region of the N gene full-length by using MEGAscript T7 Transcription Kit (ThermoFisher, Cat# AM1334), and purified with MEGAclear Transcription Clean-Up Kit (ThermoFisher, Cat# AM1908). The amplifications of qRT-PCR were performed with a CFX96 Touch Real-Time PCR System (Bio-Rad) using the following conditions: reverse transcription at 50 °C for 5 min, initial denaturation at 95 °C for 20 s, then 40 cycles of denaturing and annealing/extending at 95 °C for 3 s and 60 °C for 30 s. The lower limit of detection (LOD) was 10^{1.5} copies per reaction.

Microneutralization (MN) assay

Neutralizing antibodies were measured by a standard microneutralization (MN) assay on Vero-E6 (for ancestral and Delta strains) or VTA cells (for Omicron strain) as previously described¹⁵. The sera were heat-inactivated at 56 °C for 30 min and followed by 2-fold serial dilution, after which the diluted sera were incubated with 100 TCID₅₀ of SARS-CoV-2 virus (ancestral, Delta, and Omicron strains) for 1 h at 37 °C, respectively. The virus-serum mixtures were added to Vero-E6 or VAT cell monolayers in 96-well plates and incubated for 1 h at 37 °C. After removing the mixture, DMEM with 1% inactivated FBS was added to each well and incubated for 4 days at 37 °C for daily CPE observation. Neutralizing Ab titers are expressed as the reciprocal of the highest serum dilution preventing the appearance of CPE.

Immunizations of mice and Golden Syrian hamsters and SARS-CoV-2 challenge

Six- to eight-week-old female/male C57BL/6 mice, FcRn KO mice, and K18-hACE2 transgenic mice were intranasally (i.n.) immunized with 10 µg S-Fc, equal molar of recombinant S, or PBS in 10 µg CpG adjuvant (ODN1826, Invivogen, Cat# vac-1826-1) in a total volume of 20 µl. CpG does not increase the permeability of the airway respiratory barrier⁶⁶, and it is recognized by TLR-9 of plasmacytoid dendritic cells (pDCs) and B cells, leading to the activation of a Th1 immune response and priming the induction of long-lasting memory immune responses⁶⁷. For intramuscular (i.m.) immunizations, mice were injected bilaterally in the quadriceps femoris with a 50 µl volume containing 10 µg S-Fc antigen in 10 µg CpG. Six- to eight-week-old female/male hamsters (*n* = 6–8 per group) were vaccinated via i.n. or i.m. route with an 80 µl volume containing 30 µg S-Fc and 30 µg CpG. The mice or hamsters were boosted with the same vaccine formulations 2 or 3 weeks later.

Blood was collected from each animal 2 or 3 weeks after the boost; 3 days later, the animals were transferred to the ABSL-3+ facility for virus challenge. The K18-hACE2 mice were i.n. infected with lethal doses of SARS-CoV-2 virus in a total volume of 50 µl (2.5 × 10⁴ TCID₅₀ ancestral SARS-CoV-2 and Delta strains, or 1 × 10⁶ TCID₅₀ for Omicron strain). Due to their high susceptibility, the aged K18-hACE2 mice were challenged with 5 × 10³ TCID₅₀ ancestral strain. The hamsters were i.n. infected with 1 × 10⁵ TCID₅₀ of ancestral SARS-CoV-2 strain with a final volume of 100 µl. After infection, animals were monitored daily for morbidity (weight loss), mortality (survival), and other clinical signs of illness for 14 days. Animals losing above 25% of their body weight following infection or reaching the humane endpoint were humanely euthanized.

At the indicated time points after the virus infection, nasal washes or throat swabs were sampled to monitor the virus shedding from the upper respiratory tract. To further measure the virus replication and tissue lesion *in vivo*, 50% of the animals in each group were euthanized at 4 or 5 dpi, and different organs and tissues, including nasal turbinate, trachea, lung, brain, heart, and intestine, were harvested. The left lung lobe was fixed in a 10% neutral buffered formalin solution for histopathology analyses, while the right lung lobes and other tissues were homogenized in DMEM by Tissue Lyser (Qiagen). The homogenates were cleaned by centrifugation (16,100 × g for 10 minutes), and supernatants were collected to measure viral load.

Lung pathology

To examine the lung pathology, lungs were removed from mice in each group and fixed in 10% neutral buffered formalin solution 3 days before transferring the tissues from the ABSL-3 facility. The lungs were then paraffin-embedded, sectioned in five-micron thickness, and stained with Hematoxylin and Eosin (H & E) by Histoserv Inc (Germantown, MD). Stained lung sections were scanned using a high-definition whole-slide imaging system (Histoserv, Germantown, MD).

To determine the level of pulmonary inflammation, the lung inflammation was evaluated and scored by a board-certified veterinary pathologist blinded to the experimental design. A semi-quantitative scoring system, ranging from 0 to 5, was used to assess the following parameters: alveolitis, parenchymal pneumonia, inflammatory cell infiltration, peribronchiolitis, perivascularitis, and lung edema⁶⁸. The inflammatory scores are as follows: 0, normal; 1, very mild; 2, mild; 3, moderate; 4, marked; and 5, severe. An increment of 0.5 was assigned if the inflammatory score fell between two.

Intravascular labeling and flow cytometry

To discriminate the tissue-resident memory T cells (TRM) in the lung from the circulating T cells in the blood, the S-Fc immunized, or PBS control mice were anesthetized and intravenously injected with 3 µg of PE-CD3 Ab in 100 µl PBS through the retro-orbital route. After 5 min labeling, the treated mice were euthanized and bled. As described previously, single cells were isolated from the lung³². The lungs were perfused with 10 ml PBS, minced with scissors, and incubated in a digestion solution (RPMI with 1 mg/ml of collagenase IV, 5 mM of CaCl₂, 10 µg/ml DNase I) for 45–60 min at 37 °C on a rotating rocker. The digestion was stopped with 5 mM EDTA, and then the cells were filtered through a 70 µm cell strainer and treated with ACK buffer to lyse the red blood cells. Next, cells were purified via the 37% Percoll centrifugation to remove most epithelial cells and cell debris. After washing and resuspension with PBS, cells were stained with a Fixable Live/Dead Yellow staining dye (Invitrogen, Cat# 501121527) to differentiate between live and dead cells. Single-cell suspensions were incubated with Fc block (anti-mouse CD16/CD32, 1 µg for 1 × 10⁶ cells, BD Biosciences, Cat# 553142) at 4 °C for 30 min. After washing with FACS buffer (2% FBS and 2 mM EDTA in PBS), cells were stained with BV421-Spike tetramer (NIH tetramer center, Cat# 63745) 40 min at room temperature, then stained with FITC-CD3 Ab (BD Bioscience,

Cat# BDB555275), APC-H7-CD4 Ab (BD Bioscience, Cat#590181), BV786-CD8a Ab (Biolegend, Cat#100749), BV650-CD44 Ab (Biolegend, Cat#103049), BV421-Spike tetramer (NIH tetramer center, Cat# 63745), APC-CD69 Ab (BD Bioscience, Cat#BDB560689), and PE-eFluor10-CD103 Ab (eBioscience, Cat# 61103182) for 1 h at 4 °C. After washing, cells were fixed with 2% paraformaldehyde for 20 min and resuspended in 350 µl 1% BSA/PBS for phenotyping by FACSCelesta cytometer (BD Biosciences). Abc total antibody compensation beads (Invitrogen, Cat# A10497) and Arc amine reactive compensation beads (Invitrogen, Cat# A10346) were used to set up the compensation control. The acquired data were analyzed using the FlowJo software (Tree Star).

Airborne transmission experiments in hamsters

Airborne transmission of the SARS-CoV-2 is more efficient than fomite transmission in hamsters^{69–71}. Hence, we examined the capacity of the i.n. immunization to reduce airborne transmission of the ancestral SARS-CoV-2 between animals. The i.m. immunized hamsters were used as controls. To this end, the hamsters were either i.n. or i.m. immunized with S-Fc or left unimmunized, as described above. All hamsters were single-housed in stainless steel wire cages in an isolator, where they were grouped into donors (infected) and recipients (exposed). The isolators provided a unidirectional airflow from the donors to the recipients at an air speed of 78 L/min. The airborne transmission study was conducted following the booster. All donor hamsters at anesthesia were i.n. inoculated with 1×10^5 TCID₅₀ of SARS-CoV-2 (100 µl) and placed upstream of the airflow location in an isolator. Fourteen hours later, the recipient hamsters were placed downstream of the airflow in the same isolator. The donor and recipient cages were seated at 10 cm to avoid direct contact with animals and the effect of dust particles generated from the bedding material. After infection, the hamsters' body weight and clinical signs were monitored daily for 14 consecutive days. Throat swabs were sampled daily for 7 days in donor hamsters, while the recipient hamsters were sampled for 10 days as the onset of infection in the recipients was a few days later than that in the donors.

Statistics analysis

All data were analyzed with the Prism 9.0 software (GraphPad). The unpaired T-test (two-tailed) was used to compare the means between two groups, while one-way ANOVA was used to compare the difference if three or more groups were involved. Meanwhile, a Post Hoc test was applied after one-way ANOVA. Dunnett's multiple comparisons test was used to compare means from different treatment groups against a single control group. If the data distribution is not normal, the Mann–Whitney test (two-tailed) (for two groups) or Kruskal–Wallis test (for more than 2 groups) will be used. To compare the Kaplan–Meier survival curves, the Log-rank (Mantel–Cox) test was used. Fisher's exact test (one-tailed) was conducted to compare transmission capacities among various groups. All statistical methods used in each experiment are indicated in the Figure legends. The level of statistical significance was assigned when p values were <0.05 . The statistical significance was further classified into four levels: $p < 0.05$, $p < 0.01$, $p < 0.001$, and $p < 0.0001$.

Reporting summary

Further information on research design is available in the Nature Portfolio Reporting Summary linked to this article.

Data availability

The authors declare that all the vectors and cell lines used in this manuscript will be made available on a suitable platform. All the relevant data supporting the findings of this study are available within the Article and its Supplementary Information files or from the corresponding author on reasonable request. A Reporting Summary for this

Article is available as a Supplementary Information file. Source data are provided with this paper.

References

- V'kovski, P., Kratzel, A., Steiner, S., Stalder, H. & Thiel, V. Coronavirus biology and replication: implications for SARS-CoV-2. *Nat. Rev. Microbiol.* **19**, 155–170 (2021).
- Du, L. et al. The spike protein of SARS-CoV—a target for vaccine and therapeutic development. *Nat. Rev. Microbiol.* **7**, 226–236 (2009).
- Sakurai, A. et al. Natural history of asymptomatic SARS-CoV-2 infection. *N. Engl. J. Med.* **383**, 885–886 (2020).
- Hou, Y. J. et al. SARS-CoV-2 reverse genetics reveals a variable infection gradient in the respiratory tract. *Cell* **182**, 429–446.e14 (2020).
- Jeyanathan, M. et al. Immunological considerations for COVID-19 vaccine strategies. *Nat. Rev. Immunol.* **20**, 615–632 (2020).
- Lund, F. E. & Randall, T. D. Scent of a vaccine. *Science* **373**, 397–399 (2021).
- Tang, J. et al. Respiratory mucosal immunity against SARS-CoV-2 following mRNA vaccination. *Sci. Immunol.* **19**, eadd4853 (2022).
- Lipsitch, M., Krammer, F., Regev-Yochay, G., Lustig, Y. & Balicer, R. D. SARS-CoV-2 breakthrough infections in vaccinated individuals: measurement, causes and impact. *Nat. Rev. Immunol.* **22**, 57–65 (2022).
- Ochsner, S. P. et al. FcRn-targeted mucosal vaccination against influenza virus infection. *J. Immunol.* **207**, 1310–1321 (2021).
- Russell, M. W. & Mestecky, J. Mucosal immunity: the missing link in comprehending SARS-CoV-2 infection and transmission. *Front Immunol.* **13**, 957107 (2022).
- Spiekermann, G. M. et al. Receptor-mediated immunoglobulin G transport across mucosal barriers in adult life: functional expression of FcRn in the mammalian lung. *J. Exp. Med.* **196**, 303–310 (2002). *J. Exp. Med.* **197**, 1601 (2003).
- He, W. et al. FcRn-mediated antibody transport across epithelial cells revealed by electron tomography. *Nature* **455**, 542–546 (2008).
- Li, Z. et al. Transfer of IgG in the female genital tract by MHC class I-related neonatal Fc receptor (FcRn) confers protective immunity to vaginal infection. *Proc. Natl Acad. Sci. USA* **108**, 4388–4393 (2011).
- Roopenian, D. C. & Akilesh, S. FcRn: the neonatal Fc receptor comes of age. *Nat. Rev. Immunol.* **9**, 715–725 (2007).
- Ward, E. S., Zhou, J., Ghetie, V. & Ober, R. J. Evidence to support the cellular mechanism involved in serum IgG homeostasis in humans. *Int. Immunol.* **15**, 187–195 (2003).
- Allie, S. R. et al. The establishment of resident memory B cells in the lung requires local antigen encounter. *Nat. Immunol.* **20**, 97–108 (2019).
- Szabo, P. A., Miron, M. & Farber, D. L. Location, location, location: tissue resident memory T cells in mice and humans. *Sci. Immunol.* **4**, eaas9673 (2019).
- Letarov, A. V., Londer, Y. Y., Boudko, S. P. & Mesyanzhinov, V. V. The carboxy-terminal domain initiates trimerization of bacteriophage T4 fibrin. *Biochemistry* **64**, 817–823 (1999).
- Dekkers, G. et al. Affinity of human IgG subclasses to mouse Fc gamma receptors. *MAbs* **9**, 767–773 (2017).
- Oladunni, F. S. et al. Lethality of SARS-CoV-2 infection in K18 human angiotensin-converting enzyme 2 transgenic mice. *Nat. Commun.* **11**, 6122 (2020).
- Planas, D. et al. Considerable escape of SARS-CoV-2 Omicron to antibody neutralization. *Nature* **602**, 671–675 (2022).
- Grau-Expósito, J. et al. Peripheral and lung resident memory T cell responses against SARS-CoV-2. *Nat. Commun.* **12**, 3010 (2021).
- Sia, S. F. et al. Pathogenesis and transmission of SARS-CoV-2 in golden hamsters. *Nature* **583**, 834–838 (2020).

24. Yen, H. L. et al. Transmission of SARS-CoV-2 delta variant (AY.127) from pet hamsters to humans, leading to onward human-to-human transmission: a case study. *Lancet* **399**, 1070–1078 (2022).
25. Golden, J. W. et al. Hamsters expressing human angiotensin-converting enzyme 2 develop Severe Disease following Exposure to SARS-CoV-2. *mBio* **13**, e0290621 (2022).
26. Chandrashekar, A. et al. Vaccine protection against the SARS-CoV-2 Omicron variant in macaques. *Cell* **185**, 1549–1555.e11 (2022).
27. Wang, Q. et al. Antibody evasion by SARS-CoV-2 Omicron sub-variants BA.2.12.1, BA.4 and BA.5. *Nature* **608**, 603–608 (2022).
28. Wang, Q. et al. Alarming antibody evasion properties of rising SARS-CoV-2 BQ and XBB subvariants. *Cell* **186**, 279–286 (2023).
29. Boon, A. C. M. et al. Reduced airborne transmission of SARS-CoV-2 BA.1 Omicron virus in Syrian hamsters. *PLoS Pathog.* **18**, e1010970 (2022).
30. Nouailles, G. et al. Live-attenuated vaccine sCPD9 elicits superior mucosal and systemic immunity to SARS-CoV-2 variants in hamsters. *Nat. Microbiol.* **8**, 860–874 (2023).
31. Fischer, H. & Widdicombe, J. H. Mechanisms of acid and base secretion by the airway epithelium. *J. Membr. Biol.* **211**, 139–150 (2006).
32. Ye, L., Zeng, R., Bai, Y., Roopenian, D. C. & Zhu, X. Efficient mucosal vaccination mediated by the neonatal Fc receptor. *Nat. Biotechnol.* **29**, 158–163 (2011).
33. Lu, L. et al. A neonatal Fc receptor-targeted mucosal vaccine strategy effectively induces HIV-1 antigen-specific immunity to genital infection. *J. Virol.* **85**, 10542–10553 (2011).
34. Hartwell, B. L. et al. Intranasal vaccination with lipid-conjugated immunogens promotes antigen transmucosal uptake to drive mucosal and systemic immunity. *Sci. Transl. Med.* **14**, eabn1413 (2022).
35. Sterlin, D. et al. IgA dominates the early neutralizing antibody response to SARS-CoV-2. *Sci. Transl. Med.* **13**, eabd2223 (2021).
36. Hassan, A. O. et al. A single-dose intranasal ChAd vaccine protects upper and lower respiratory tracts against SARS-CoV-2. *Cell* **183**, 169–184.e13 (2020).
37. Afkhami, S. et al. Respiratory mucosal delivery of next-generation COVID-19 vaccine provides robust protection against both ancestral and variant strains of SARS-CoV-2. *Cell* **185**, 896–915.e19 (2022).
38. Zhou, D. et al. Robust SARS-CoV-2 infection in nasal turbinates after treatment with systemic neutralizing antibodies. *Cell Host Microbe* **29**, 551–563.e5 (2021).
39. Wellford, S. A. et al. Mucosal plasma cells are required to protect the upper airway and brain from infection. *Immunity* **55**, 2118–2134 (2022).
40. van Doremalen, N. et al. Intranasal ChAdOx1 nCoV-19/AZD1222 vaccination reduces viral shedding after SARS-CoV-2 D614G challenge in preclinical models. *Sci. Transl. Med.* **13**, eabh0755 (2021).
41. Zeng et al. SARS-CoV-2 spreads through cell-to-cell transmission. *Proc. Natl Acad. Sci. USA* **119**, e2111400119 (2022).
42. Mackin, S. R. et al. Fc-γR-dependent antibody effector functions are required for vaccine-mediated protection against antigen-shifted variants of SARS-CoV-2. *Nat. Microbiol.* **8**, 569–580 (2023).
43. Dan, J. M. et al. Immunological memory to SARS-CoV-2 assessed for up to 8 months after infection. *Science* **371**, eabf4063 (2021).
44. Fröberg, J. et al. SARS-CoV-2 mucosal antibody development and persistence and their relation to viral load and COVID-19 symptoms. *Nat. Commun.* **12**, 5621 (2021).
45. Roukens, A. H. E. et al. Prolonged activation of nasal immune cell populations and development of tissue-resident SARS-CoV-2-specific CD8⁺ T cell responses following COVID-19. *Nat. Immunol.* **23**, 23–32 (2022).
46. Baker, K. et al. Neonatal Fc receptor for IgG (FcRn) regulates cross-presentation of IgG immune complexes by CD8-CD11b⁺ dendritic cells. *Proc. Natl Acad. Sci. USA* **108**, 9927–9932 (2011).
47. Liu, X. et al. The neonatal FcR-mediated presentation of immune-complexed antigen is associated with endosomal and phagosomal pH and antigen stability in macrophages and dendritic cells. *J. Immunol.* **186**, 4674–4686 (2011).
48. Oh, J. E. et al. Intranasal priming induces local lung-resident B cell populations that secrete protective mucosal antiviral IgA. *Sci. Immunol.* **6**, eabj5129 (2021).
49. Yoshida, M. et al. Human neonatal Fc receptor mediates transport of IgG into luminal secretions for delivery of antigens to mucosal dendritic cells. *Immunity* **20**, 769–783 (2004).
50. Sui, Y. et al. Protection against SARS-CoV-2 infection by a mucosal vaccine in rhesus macaques. *JCI Insight* **6**, e148494 (2021).
51. Mao, T. et al. Unadjuvanted intranasal spike vaccine elicits protective mucosal immunity against sarbecoviruses. *Science* **27**, eabo2523 (2022).
52. Al-Aly, Z., Bowe, B. & Xie, Y. Long COVID after breakthrough SARS-CoV-2 infection. *Nat. Med.* **28**, 583–590 (2022).
53. Meinhardt, J. et al. Olfactory transmucosal SARS-CoV-2 invasion as a port of central nervous system entry in individuals with COVID-19. *Nat. Neurosci.* **24**, 168–175 (2021).
54. Bauer, L. et al. The neuroinvasiveness, neurotropism, and neurovirulence of SARS-CoV-2. *Trends Neurosci.* **SO166-2236**, 00050–00059 (2022).
55. Andrews, M. G. et al. Tropism of SARS-CoV-2 for human cortical astrocytes. *Proc. Natl Acad. Sci. USA* **119**, e2122236119 (2022).
56. Hunter, P. Viral diseases and the brain: Long COVID puts the spotlight on how viral infections affect the brain. *EMBO Rep.* **23**, e54342 (2022).
57. McCray, P. B. Jr. et al. Lethal infection of K18-hACE2 mice infected with severe acute respiratory syndrome coronavirus. *J. Virol.* **81**, 813–821 (2007).
58. Pallesen, J. et al. Immunogenicity and structures of a rationally designed prefusion MERS-CoV spike antigen. *Proc. Natl Acad. Sci. USA* **114**, E7348–E7357 (2017).
59. Walls, A. C. et al. Structure, function, and antigenicity of the SARS-CoV-2 spike glycoprotein. *Cell* **181**, 281–292 (2020).
60. Nimmerjahn, F. & Ravetch, J. V. Divergent immunoglobulin g subclass activity through selective Fc receptor binding. *Science* **310**, 1510–1512 (2005).
61. Idusogie, E. et al. Mapping of the C1q binding site on rituxan, a chimeric antibody with a human IgG1 Fc. *J. Immunol.* **164**, 4178–4184 (2000).
62. Reed, L. J. & Muench, H. A simple method of estimating fifty per cent endpoints. *Am. J. Epidemiol.* **27**, 493–497 (1938).
63. Matsuyama, S. et al. Enhanced isolation of SARS-CoV-2 by TMPRSS2-expressing cells. *Proc. Natl Acad. Sci. USA* **117**, 7001–7003 (2020).
64. Dagotto, G. et al. Comparison of subgenomic and total RNA in SARS-CoV-2 challenged rhesus macaques. *J. Virol.* **95**, e02370–20 (2021).
65. Li, D. et al. In vitro and in vivo functions of SARS-CoV-2 infection-enhancing and neutralizing antibodies. *Cell* **184**, 4203–4219 (2021).
66. Kubo, T. et al. CpG-DNA enhances the tight junction integrity of the bronchial epithelial cell barrier. *J. Allergy Clin. Immunol.* **136**, 1413–6.e1-8 (2015).
67. Bode, C., Zhao, G., Steinhagen, F., Kinjo, T. & Klinman, D. M. CpG DNA as a vaccine adjuvant. *Expert Rev. Vaccines* **10**, 499–511 (2011).
68. Imai, M. et al. Syrian hamsters as a small animal model for SARS-CoV-2 infection and countermeasure development. *Proc. Natl Acad. Sci. USA* **117**, 16587–16595 (2020).
69. Port, J. R. et al. SARS-CoV-2 disease severity and transmission efficiency is increased for airborne compared to fomite exposure in Syrian hamsters. *Nat. Commun.* **12**, 4985 (2021).

70. Chen, Y. et al. Age-associated SARS-CoV-2 breakthrough infection and changes in immune response in a mouse model. *Emerg. Microbes Infect.* **11**, 368–383 (2022).
71. Lyke, K. E. et al. Rapid decline in vaccine-boosted neutralizing antibodies against SARS-CoV-2 Omicron variant. *Cell Rep. Med.* **3**, 100679 (2022).

Acknowledgements

We are grateful to BEI Resources for supplying us with the SARS-CoV-2 virus and its variants, cells, and antibodies. We thank Dr. Chinta Lamichhane, who shared the sera from the convalescent COVID-19 patients and healthy persons. We are most grateful for the technical help from Ms. Ely Elena Guevara and Mr. Takele Yazew. This work was partly supported by NIH grants A1146063, A1130712 (X.Z.), and MAES grants from the University of Maryland (X.Z.). The Basil and Anne Hatzios Scholarship Fund for Veterinary Medical Research supports Zizhen (Jenny) Miao. The intramural research program of the USDA ARS supports W.T., A. R., and A. K.

Author contributions

W.L. and X.Z. designed experiments and analyzed data. W.L., W.T., and X.Z. wrote the paper. W.L., T.W., A.R., Z.M., B.P.V., H.Y., G.A., B.D., A.K., and T.L. conducted experiments. W.T. provided critical materials, interpreted data, and made editorial suggestions.

Competing interests

X.Z. is listed as an inventor of the patent: US Patent 9,238,683 B2, issued on Jan. 19, 2016, entitled “Efficient Mucosal Vaccination Mediated by the Neonatal Fc Receptor.” X.Z., W.L., and T.W. are listed as inventors on the following patent applications: U.S. Nonprovisional Patent Application No. 20220098242, filed on February 26, 2021, entitled “Compositions and methods for mucosal vaccination against SARS-CoV-2”. U.S. Provisional Application No.: 63/267782, filed on February 8, 2022, “Systems and Methods for FcRn-targeted Nasal Vaccination.” The remaining authors declare no competing interest.

Additional information

Supplementary information The online version contains supplementary material available at <https://doi.org/10.1038/s41467-023-42796-0>.

Correspondence and requests for materials should be addressed to Xiaoping Zhu.

Peer review information *Nature Communications* thanks the anonymous reviewers for their contribution to the peer review of this work. A peer review file is available.

Reprints and permissions information is available at <http://www.nature.com/reprints>

Publisher’s note Springer Nature remains neutral with regard to jurisdictional claims in published maps and institutional affiliations.

Open Access This article is licensed under a Creative Commons Attribution 4.0 International License, which permits use, sharing, adaptation, distribution and reproduction in any medium or format, as long as you give appropriate credit to the original author(s) and the source, provide a link to the Creative Commons license, and indicate if changes were made. The images or other third party material in this article are included in the article’s Creative Commons license, unless indicated otherwise in a credit line to the material. If material is not included in the article’s Creative Commons license and your intended use is not permitted by statutory regulation or exceeds the permitted use, you will need to obtain permission directly from the copyright holder. To view a copy of this license, visit <http://creativecommons.org/licenses/by/4.0/>.

© The Author(s) 2023